ADDIS ABABA UNIVERSITY

ADDIS ABABA INSTITUTE OF TECHNOLOGY

SCHOOL OF MECHANICAL AND INDUSTRIAL ENGINEERING

Modeling of Geometric Pore Parameters for the Sintered Matrix (Fe-0.85Mo-0.35C) to Study the Effect of Pore Size and Shape on Elastic properties of Steels

A thesis Submitted to the graduate school of Addis Ababa University in Partial fulfillment of the Requirements for the Degree Master of Science in Mechanical Engineering (Mechanical Design)

By: Fentahun Yihunie

Advisor: Dr. Samuel Tesfaye

Addis Ababa, Ethiopia
July, 2023

Declaration

I declare that this work which is being presented in this thesis entitled with "**Modeling of Geometric Pore Parameters for the Sintered Matrix (Fe-0.85Mo-0.35C) to Study the Effect of Pore Size and Shape on Elastic properties of Steels"** is the original work of mine where all the work carried out as input according to my knowledge under the supervision of Dr. Samuel Tesfaye. The overall work compiles with the regulation of the university and has not been previously submitted for a degree at any higher educational institutions.

Fentahun Yihune Zegeye _____ _____

Name of Candidate Signature Date

This is to certify that the above declaration made by the candidate is correct to the best of my knowledge.

Samuel Tesfaye (PhD) _____ July 05, 2023

Advisor Signature Date

Addis Ababa University

Addis Ababa Institute of Technology

School of Mechanical and Industrial Engineering

Modeling of Geometric Pore Parameters for the Sintered Matrix (Fe-0.85Mo-0.35C) to Study the Effect of Pore Size and Shape on Elastic properties of Steels

By: Fentahun Yihunie Zegeye

Approved by Board of Examiners:

Samuel Tesfaye (PhD)	_____	July 05, 2023
Advisor	Signature	Date
Araya Abera (PhD)	_____	_____
Internal Examiner	Signature	Date
Haileleoul Sahle (PhD)	_____	_____
External Examiner	Signature	Date
Araya Abera (PhD)	_____	_____
SMIE Dean	Signature	Date
Sosina Mengistu (PhD)	_____	_____
Postgraduate Director	Signature	Date

ACKNOWLEDGMENTS

I am profoundly grateful to my advisor, Assistant Professor Samuel Tesfaye (PhD), for his energetic support and encouragement, and his valuable guidance and day to day advice throughout this research project. I would also like to express my appreciation to him for providing me the opportunity to carry out this research work.

And I would like to express my gratitude to all those who support me in accomplishing this thesis.

Last, but not least, I simply could not have come this far without love, understanding, patience, and inspiration from my wife, Yenewub Nehabie.

Abstract

Porosity is a void and inherent characteristic of powder metallurgy (PM) material. This thesis work is modeling of representative volume element (RVE) microstructures with square, triangular and rectangular pore shape with different circularity and study the effect of pore shape and pore parameters on material properties for the Sintered steel (Fe-0.85Mo-0.35C) using finite element method (FEM). Solidwork and Digimat were used to model RVE microstructure and ABAQUS to simulate the process. A parametric study is conducted to investigate the effect of neck radius of curvature (R'=0, R'=0.5, R'=1 and R'=1.5), equivalent diameter, circularity and fraction of load bearing section. The low circularity is determined pore which is 0.21, and the high circularity is determined for circularity pore (1). The low circularity 0.21 yield strength is 348.55 M_{Pa} and high circularity of 1 yield strength is 719.24 M_{Pa}. Besides, sharpness of pore, triangular pore has good yield strength than square and rectangular pore. For the effect of neck radius of curvature (R' = 0) square pore have high elastic modulus (160.98 G_{pa}) and triangular pore have low elastic modulus (147.68 G_{pa}). And (R' = 1.5) triangular pore have high elastic modulus (176.2 G_{pa}). With circularity of pore from all pore model triangular have low circularity of 0.21 with low elastic modulus of 147.68 G_{pa} and high circularity of 1 with high elastic modulus 184.75 G_{pa}. There is high equivalent diameter in rectangular pore of with low elastic modulus (149.84 G_{pa}) and low in triangular pore with high elastic modulus (184.75 G_{pa}). RVE Microstructure with 8 % square triangular and rectangular pore shows direct relationship between the circularity, neck radius of curvature and fraction of load bearing with the mechanical properties of the material. And inverse relationship between pore size and mechanical properties of material.

Key words: pore shape, neck radius of curvature, pore parameters, fraction of load bearing, mechanical properties

List of Table

List of Figures

List of tables

List of Symbols and Abbreviations

Symbol	Description	Unit
E	Yonge's modulus	G_{Pa}
ρ	Density	Kg/M^3
σ_y	Yield strength	M_{Pa}
Φ	Load bearing section	
ν	Poisons ratio	
A_P	Pore Area	mm^2
V	Volume	mm^3
d	diameter	mm
R	radius	mm
P_P	Pore perimeter	mm
ε	Porosity	
α	alpha	
θ	theta	
β	beta	
f_{cir}	Pore circularity	
D_{eq}	Equivalent diameter	
R	neck radius	mm
a	particle radius	mm
P	Applied pressure	M_{Pa}

Abbreviation	**Description**
RVE	Representative Volume element
B. C	Boundary condition
PM	Powder Metallurgy
FEA	Finite Element Analysis
FEM	Finite Element method
μm	Micrometer
CAE	Complete Abaqus Environment
CAD	Computer Aided Design
FE	Finite Element
EVA	Ethylene-co-Vinyl Acetate
PMMA	Poly methyl methacrylate

CHAPTER ONE

INTRODUCTION

1.1 Background

Powder metallurgy (PM) is a metal processing technology in which parts are produced from metallic powders. In the usual PM production sequence, the powders are compressed into the desired shape and then heated to cause bonding of the particles into a hard, rigid mass. Compression, called pressing, is accomplished in a press-type machine using tools designed specifically for the part to be manufactured [3]. The tooling, which typically consists of a die and one or more punches, can be expensive, and PM is therefore most appropriate for medium and high production. The heating treatment, called sintering, is performed at a temperature below the melting point of the metal [4].

Powder metallurgy (PM) has proven to be an effective technique for manufacturing a variety of complex-shaped steel parts with accurate and reproducible dimensions, low cost, high performance and ability to be processed to net or at least near-net shape [4]. Higher relative density is one of the most important factors for producing high quality PM parts, since the density strongly influences the physical and mechanical properties [5].

Pinions, gears, bearings, cams, Cranks, Roller, ring, O ring Seal, bearing cages, Housings, Light bulb filaments, Sprinkler mechanisms are among the mechanical components produced by powder metallurgy [14]. Porosity is the inherent characteristic of the microstructure of these components that are processed by powder compaction and subsequent sintering processes [15]. To evaluate their resistance to mechanical loading, characterization of pore parameters, such as size, distribution, and the shape is required to incorporate its effect on the stress distributions [16].

Porous sintered steels have lower mechanical properties than the corresponding full dense steels with the same matrix and micro hardness because of its porosity [6]. Pores reduce the resisting section and cause local stress accumulation, so that they act as sites for crack nucleation. Moreover, they constitute a favorable path for crack propagation. The effect of porosity on the

mechanical properties depends on the following factors: the quantity of pores (i.e., the fractional porosity); their interconnection; size; morphology; and distribution [8].

In powder metallurgy the parts produced by this route are characterized by porosity. Porosity represents the open volume of a powder metallurgy components after sintering [26]. It is difficult to carry out a piece of powder metallurgy without porosity, even after sintering [28].

The porosity in Powder Metallurgy parts is correlated to processing parameters such as green density, alloying elements, particle size distribution of the powders, sintering temperature and time. Porosity is an important parameter because is affecting the mechanical properties of these materials [18]. Pores have been proposed to act as crack propagation through the pore surface. In many studies, crack initiation occurred due to pores or groups of pores located at or near the sample surface. The additions of different amounts of alloying elements have influence on microstructures and mechanical properties of the parts produced by powder metallurgy [27].

Sintering ferrous powder metallurgy components have emerged as attractive candidates for replacing wrought alloys in many applications due to their low-cost high performance and ability to be processed approximate to net shape [14]. Sintering materials are typically characterized by residual porosity after sintering. The nature of porosity is controlled by several processing parameters such as green density sintering temperature and time, addition of alloys and particle size of the initial powders. In particular the shape, size, circularity, fraction, distribution and morphology of the porosity have a profound effect on mechanical properties [14].

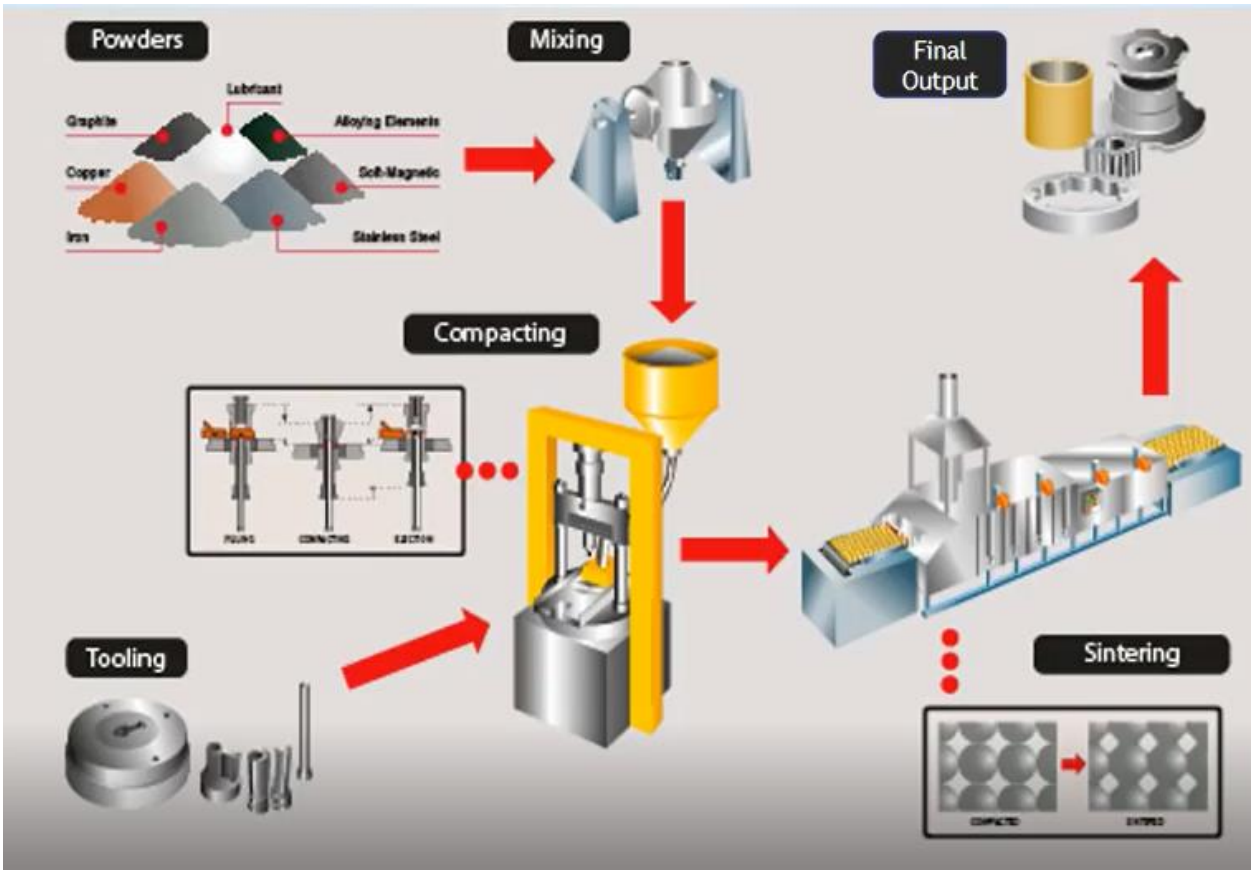

Figure 1.1 Powder Metallurgy Manufacturing Process and formation of pore [16]

Figure 1.1 describes the production process of equipment's, tools or products in powder metallurgy process and formation of pore in sintered matrix. Several spherical metal powders were fabricated successfully by using the high-temperature re melting spheroidization (HRS) technology [6].

Green compacts are usually compacted from multiple powders, which include both hard particles to construct the skeleton and soft particles to bind the skeleton. In the cold compaction of the multiple powders mixture, the pore size in the green compacts is mainly affected by the size and the shape of the hard particles in these powder mixtures [24].

The size of pores is affected by the both of the size of hard particles and the compaction pressure in the cold densification process. However, the effects of compaction pressure on pore size in cold densification are very limited when the pressure reaches a threshold value. Pore size in green compacts can be lowered by lowering the size of the hard particles in the multiple powder mixture [20].

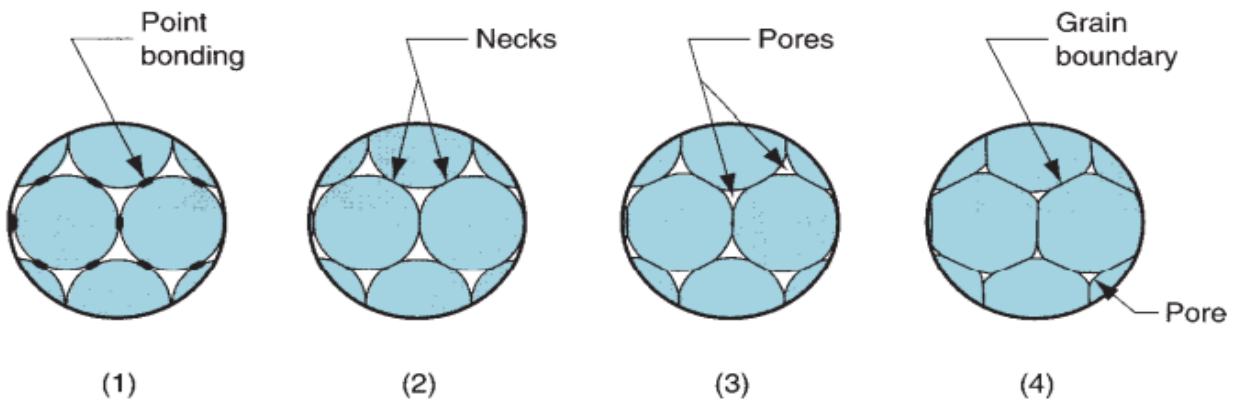

Figure 1.2 Sintering on a microscopic scale [14]

1) particle bonding is initiated at contact points;
2) contact points grow into "necks";
3) the pores between particles are reduced in size; and
4) Grain boundaries develop between particles in place of the necked regions.

1.2 Sintered Steel

Particles embedded in a matrix are commonly encountered in metal matrixes since they arise during melt processing by non-controlled phase changes, mechanical interaction of the melt with its surroundings, or they are added intentionally as filler material [20]. Stiff and soft particle inclusions in a matrix have effects that could be considered adverse or beneficial in the physical and mechanical properties of the bulk matrix [19].

1.3 Porosity

Porosity is empty space in a material. Pores are important characteristics in powder metallurgy alloy parts. The effect of processing parameters effect on pore size [16]. If pore size can be controlled as small as several or tens of nanometers in PM alloy parts, the parts may gain special physical or mechanical properties. The challenge to obtain pores sizing in several or tens of nanometers in PM alloy parts [14].

Pores are formed in compaction process of green compacts, and then coalesce or shrink in sintering. Pores are main characteristics of powder metallurgy alloy parts [17]. These parts gain

certain kind of properties due to the presence of pores inside. Thus, materialists are trying to control the shape, the size and the distribution of pores in the PM parts [18].

Porosity roughly represents the fraction of void volume over total volume. Pore structures like pore size, morphology and distribution of porosity within the pressed part present critical items in the load-bearing sections. The load bearing has a large influence on the mechanical properties [16].

Porosity, in Powder Metallurgy matrix, can reduced material resistance to deformation, nucleation and propagation of cracks, and variable should be incorporated into the material response predicting models through pore parameters (pore circularity, pore shape and equivalent diameter) [15].

There are many types of pore shape like:

Square pore shape: formed between four particles.

Triangular pore shape: formed between three particles.

Rectangular pore shape: formed between four particles. And like circular, irregular etc. pore shape.

a) b)

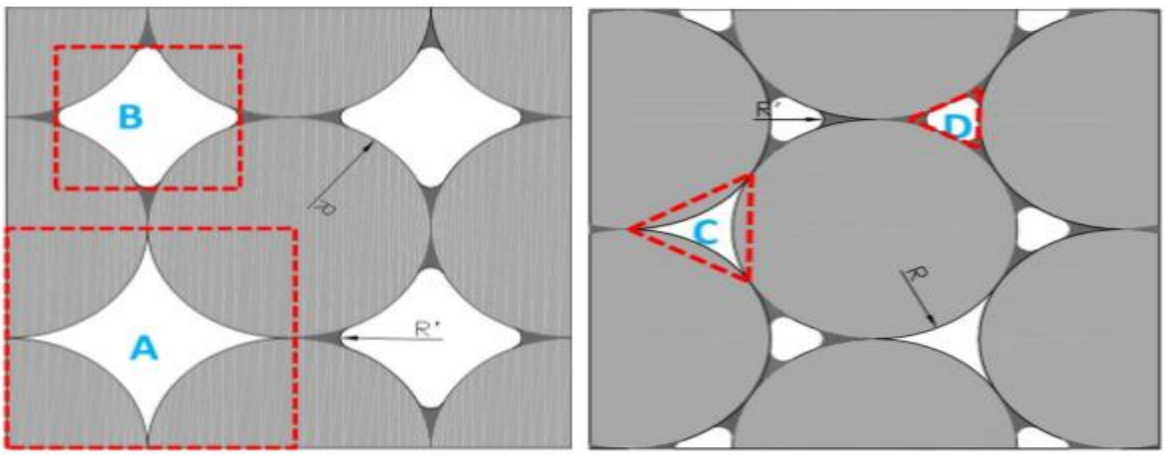

c) d)

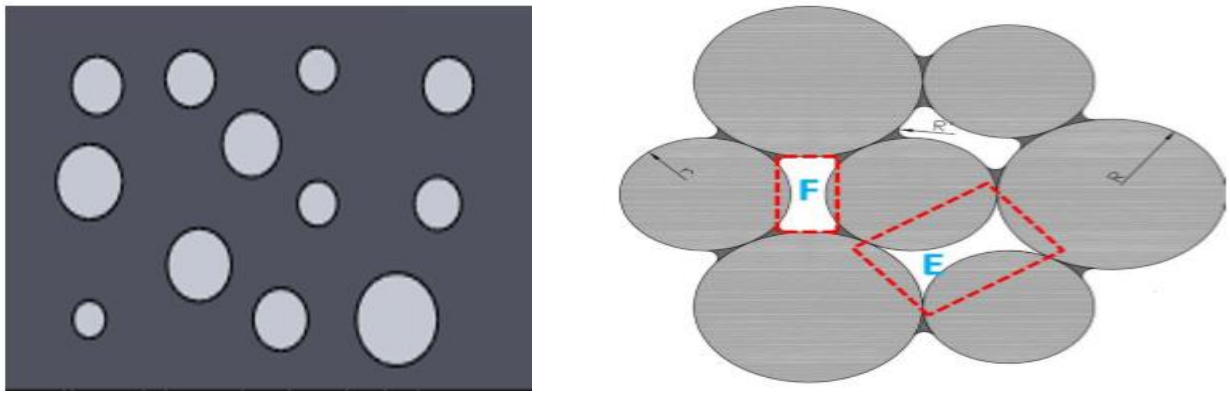

Figure 1.3 a) square, b) triangular, c) circular and d) rectangular pore shapes

Interconnected porosity causes an increase in the localization of strain at relatively smaller sintered regions between particles, while isolated porosity results in more homogeneous deformation. It is also not uncommon for the porosity distribution in the material to be in homogeneous. In this case, strain localization will take place at pore clusters [7].

Fraction of porosity, pore size, pore shape, and pore spacing are all important factors that control the fatigue behavior of PM materials [11]. In general, more irregular pores have a higher stress than perfectly round pores. Pores have also been shown to act as linkage sites for crack propagation [8].

1.4 Statement of the Problem

Porosity is one of the major defects in Powder metallurgy. Porosity formed in the product will decrease the mechanical performance of the material significantly. For example, porosity degrades properties like young's modulus and tensile strength. Thus, it is important to know when porosity forms and how to minimize the negative effects. A lot of researches have been conducted on the effect of circular and spherical pore shapes on properties of material using experimental, analytical and numerical methods. And some researchers study the effect of volume fraction of porosity on material properties using experimentally characterizing microstructures and processing the image to relate the property with porosity. However, the effect of rectangular, triangular, and square pore shapes on the effect of properties of material have not yet studied. In this thesis the effect of rectangular, triangular, and square pore shapes

with different neck radius of square, rectangular and triangular on the effect of properties have been studied using finite element method.

1.5 Objectives

1.5.1 General Objectives

The main objective of this study is modeling of rectangular, triangular, and square pore shapes to study the effect of pore parameters on the effect of material properties for the sintered steel Fe-0.85Mo-0.35C using Solidwork, Digimat and Abaqus softwares.

1.5.2 Specific objectives

- Develop 3D model with square, rectangular and triangular pore shapes to study the pore parameters, such as circularity, equvelent diameter and load bearing surface.
- Study the effect of square, rectangular and triangular pores and their parameters on material properties of yield strength.
- Compare the effect of triangular, rectangular and square pore shapes on yield strength.
- Study the effect of pore parameters on mechanical properties of elastic modulus.

1.6 Scope of the study

This study deals the effect of pore shapes such as triangular, square, and rectangular on the material properties using finite element method. Yield strength will be determined, and the variation of influential parameters such as R', Deq, f_{cir} and Φ and pore shape on material properties will be investigated. Lastly, this study will compare the effect of pore parameters and shape on material properties of porous materials of sintered steel Fe-0.85Mo-0.35C.

1.7 Limitation of the study

This work will not consider the exact position of pore and distance between the pore because it is impossible to predict the exact position and distance between the pore in Digimat software. In this study the pore in RVE microstructure is placed by randomly and finely. The analysis will be limited to homogeneous in property and isotropic materials.

1.8 Structure of Thesis

The entire research work presented in this thesis can be covered by five chapters, as detailed below.

Chapter 1 is an introduction to this thesis, indicating the problem statement, objectives of this thesis, scope, limitation, and organization of this thesis.

Chapter 2 covers an extensive literature review of the effect of pore parameters, size, shape and volume fraction on material properties in analytical, experimental and finite element methods.

Chapter 3 describes the mechanical properties of RVE materials. As well as the modeling and FEA simulation procedure of RVE microstructure using solidwork, Digimat and abaqus.

Chapter 4 presents the associated simulation result and discussion. Analyses of the stress and strain with different pore parameters. Study the effect of pore shape and size on material properties.

Chapter 5 conclusion and recommendation drawn from this thesis.

CHAPTER TWO

LITRATURE REVIEW

2.1 porous sintered steels

Sintered ferrous powder metallurgy (PM) components have emerged as attractive candidates for replacing wrought alloys in many applications, due to their low cost, high performance, and ability to be processed to near-net shape. Sintered materials are typically characterized by residual porosity after sintering, which is quite detrimental to the mechanical properties of these materials [11-14].

The nature of the porosity is controlled by several processing variables such as:

- Green density,
- Sintering temperature and time,
- Alloying additions, and
- Particle size of the initial powders.

In particular, the fraction, size, distribution, and morphology of the porosity have a profound impact on mechanical behavior [14].

Under monotonic tensile loading, porosity reduces the effective load bearing cross-sectional area and acts as a stress concentration site for strain localization and damage, decreasing both strength and ductility [12]. In general, the porosity in sintered ferrous alloys is bimodal in nature and can be divided into primary or secondary porosity. Primary porosity consists of larger pores, owing primarily to the powder packing characteristics, which result in less than complete densification during sintering. Secondary porosity, on the other hand, consists of much smaller pores, often caused by the transient liquid phase of one or more alloying additions that form during sintering [18].

2.1.1 Evolution of Pore Structure

In sintered steels, the porosity depends on one hand on the compacting pressure, which, combined with the compatibility of the starting powder mix, defines the total porosity, and on the

other hand on the sintering process which defines the pore morphology, usually represented by shape factors and, within a certain porosity range, the connectivity as well [14].

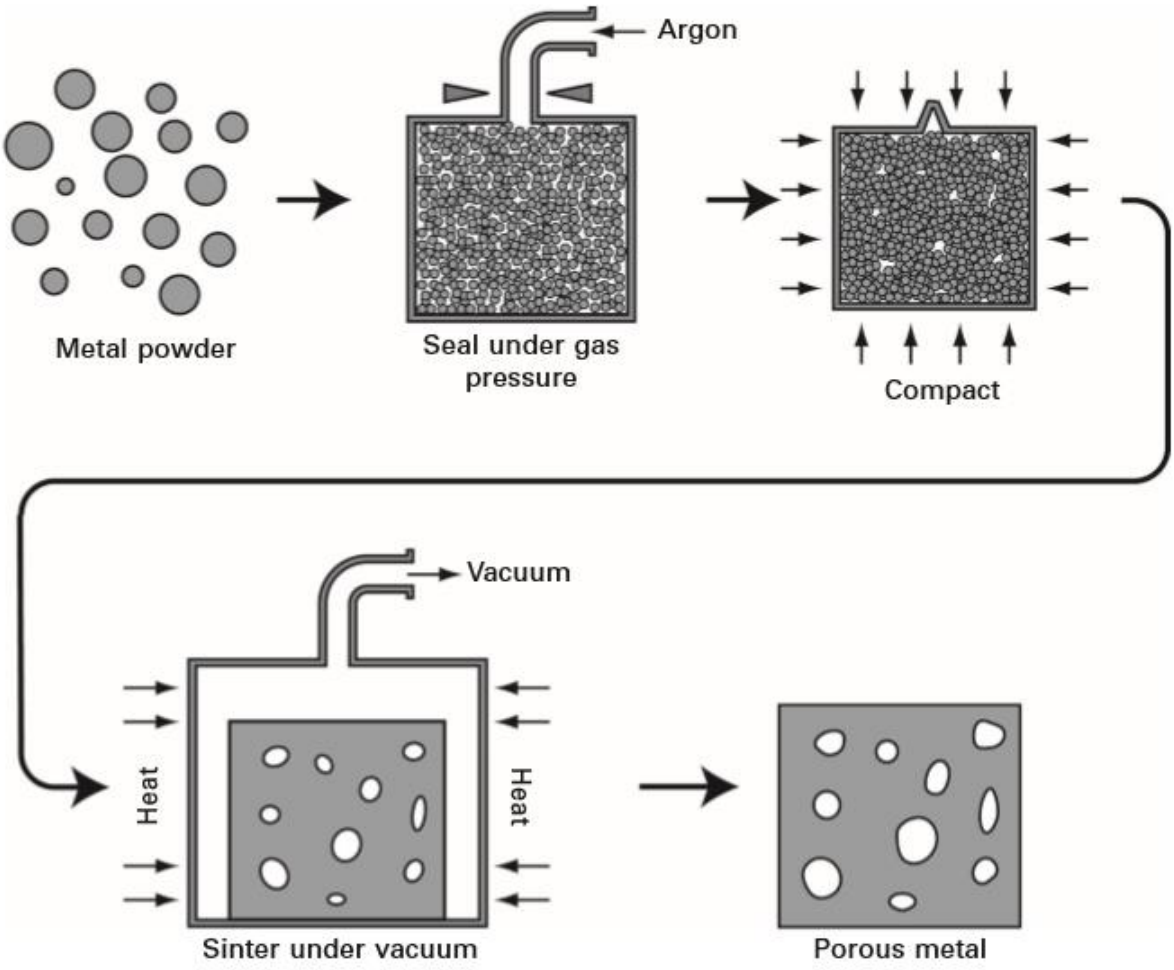

Figure 2.1 Schematic diagram of process for porous sintering steel [14]

The pores are virtually interconnected and open to the surface, as they are in the initial state, for example, in dew axed green compact. At higher density levels, however, the pore channels linking the triple junctions tend to become smaller and smaller, and if intense sintering is applied, these channels are closed and the triple junctions remain as isolated pores [28].

2.1.2 Pore Shape

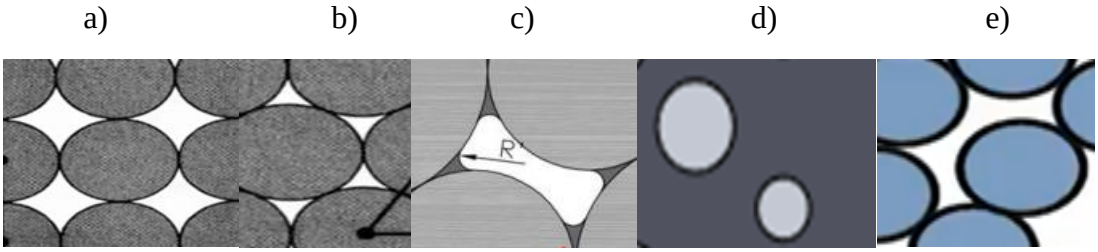

Figure 2.2 a) square, b) triangular, c) rectangular d) circular and e) irregular pore shapes

Square pore shape: formed between four equal particles.

Triangular pore shape: formed between three equal particles.

Rectangular pore shape: formed between four particles. The two parallel sides equal each other.

Circular pore shape: formed by highly compacted and sainted.

Irregular pore shape: formed by loosely packed and sorting.

Mosely square, rectangular, triangular and circular pore were formed.

2.2 Modeling of Pore Parameters

Analytical modeling of pore geometry in porous material was complex due to the diversity of pores shapes and sizes. According to the classical model, a sharp neck is created between two perfect spherical particles (represents the initial stage of the sintering) gradually shrinkage it becames round, and from the geometry, the ratio of neck to particle size is related by $x/a > 0.3$, where X is neck radius size and a is the particle radius size [4]. Figure 3.2 illustrates the proposed pore models that are defined by the spaces between spherical particles.

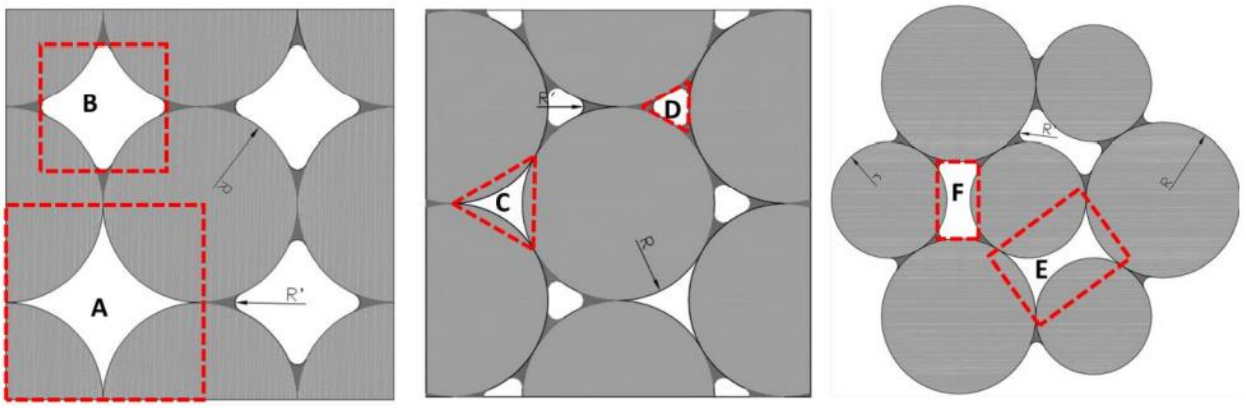

Figure 2.3 Three types of pore models: square (A, B), triangular (C, D) and rectangular (E, F) [1]

The pore geometries, highlighted in the red in figure 3.2, are voids that are defined based on the number of contacts between spherical particle size. These six pore geometries are characterized as follows:

- ✓ A and B are square geometric pores formed between four equal particles (it radius is R) with sharp (R'= 0) and rounded (R' > 0) edge, respectively;
- ✓ C and D are triangular pores formed between three equal particles (it radius is R) with sharp (R'= 0) and rounded (R'> 0) edge, respectively;
- ✓ E and F are rectangular geometric pores formed between different sized particles (its radius are R and r) with sharp (R'= 0) and rounded (R'> 0) edge, respectively.

Three pore models as a square, triangular and rectangular geometries were defined in both cases of sharp and rounded edges. A sharp-edged pore model is, which is the simplest one, formed when the particles undergo a point contact, or the radius (R') of the rounded edge is zero, and the size and shape of the three pore models vary with R and R' [1]. The modes can be defined based on those dimensions except for rectangular geometries formed between particles with different sizes (R and r), which requires an additional characteristic that is the gap between particles of similar sizes. The pore parameters (f_{circle}, D_{eq} and Φ) are always less than 1 unless otherwise, all pore are perfect circles, which is not mostly realistic in PM microstructures. Circular pore morphology is the desired microstructures of PM materials because it provides good mechanical properties than other pores [1].

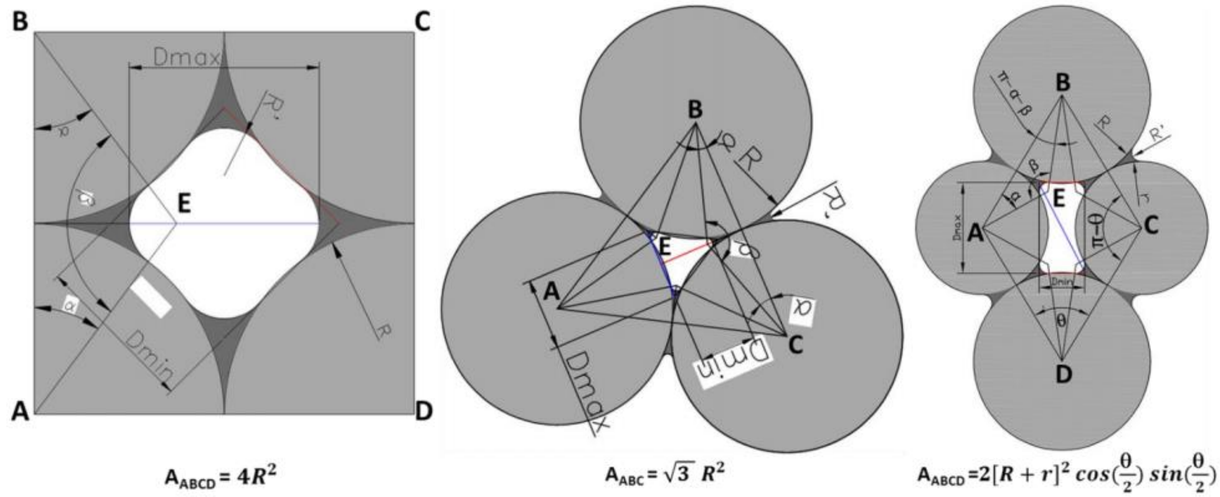

Figure 2.4 Geometrical relation of pores and circumscribed geometries [1]

The area of the square geometric pore (R'=0) valuated by subtracting the area of four circular sectors (characterized by the radius R and angle 90^0) from an area of square ABCD. Area of the square geometric pore with the sharp neck ($A_{sharp\ neck,\ squ}$) is given by Eq.1.

$$A_{sharp\ neck,\ squ} = (4-\pi)R^2 \quad \ldots [1]$$

Area of the triangular geometric pore with the sharp neck ($A_{sharp\ neck,\Delta}$) evaluated by subtracting the area of three circular sectors (characterized by the radius R and angle 60^0) from an area of a bigger equilateral triangle ABC and is given by Eq. 2.

$$A_{sharp\ neck,\Delta} = (\sqrt{3}-\frac{\pi}{2})R^2 \quad \ldots [2]$$

Area of the rectangular geometric pore with the sharp neck ($A_{sharp\ neck,\ \square}$) evaluated by subtracting the area of four circular sectors (characterized by the radius R/r and angles θ/π- θ) from an area of rhombus ABCD is given by Eq. 3.

$$A_{sharp\ neck,\ \square} = 2(R+r)^2 \cos\left(\frac{\theta}{2}\right) \sin\left(\frac{\theta}{2}\right) - r^2(\pi-\theta) - R^2\,\theta \quad \ldots [3]$$

Figure 2.5 illustrates the triangles ABE constructed from the square, triangular, and rectangular geometric pore. with a side length of R+r, r+R', and R+R'. When the particle size is the same

such as, R=r, square and rectangular geometric pore is the same. A_3 (grown neck area between particles) should be excluded from the rounded neck pore model by subtracting from the area of sharp neck pore.

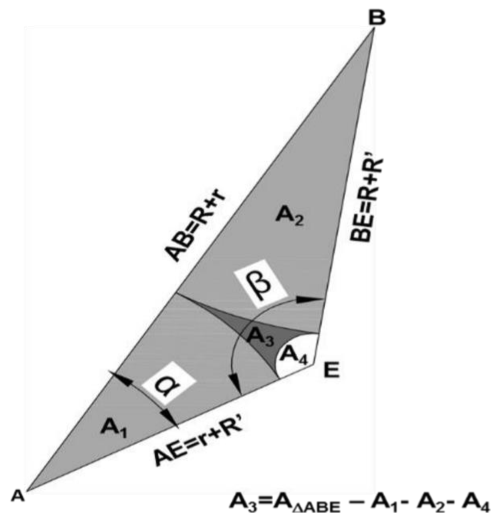

Figure 2.5 Triangle ABE and its vertices are at the centers of particles and neck curvature

The pore geometries and dimensions mathematically correlated with the particle and neck size using

Heron's formula and cosine rules. The angles of triangle ABE calculated from Eq. 4 and Eq. 5 (cosine rule).

$$\cos\alpha = \frac{AE^2+AB^2-BE^2}{2AE\times AB} \quad \ldots\ldots\ldots\ldots\ldots\ldots\ldots\ldots\ldots\ldots [4]$$

$$\cos\beta = \frac{AE^2+BE^2-AB^2}{2AE\times BE} \quad \ldots\ldots\ldots\ldots\ldots\ldots\ldots\ldots\ldots\ldots [5]$$

Area of triangle (A_{ABE}) is given by Eq.7 (Heron's formula).

$$A_{\Delta ABE} = \sqrt{\mathrm{P(P - AB)(P - AE)(P - BE)}} \quad \ldots\ldots\ldots\ldots\ldots\ldots\ldots\ldots [6]$$

Where P is the semi perimeter of the triangle and it is given by P = 2R + R' for square and triangular pore and P = R + r + R' for rectangular pore model.

A_3 (as described by Figure 3.5) was evaluated using Eq. 8.

$$A_3 = \begin{cases} R\sqrt{2RR' + R'^2} - \frac{R'^2(\pi - 2\alpha)}{2} - R^2\alpha, & square\ or\ triangular\ pore \\ \sqrt{RrR'(R + r + R')} - \frac{R^2(\pi - \alpha - \beta)}{2} - \frac{R'^2\beta}{2} - \frac{r^2\alpha}{2}, & Rectangular\ pore \end{cases} \quad \ldots\ldots\ldots\ldots\ldots\ldots\ldots [7]$$

Therefore, the area of square/rectangular pore with rounded neck ($A_{\text{round neck, }\square}$)can be evaluated by subtracting 4 times of A_3 from the total area of the pore with a sharp neck (Eq.1) and is given by Eq. 7.

$$A_{\text{round neck, }\square} = A_{\text{sharp neck, }\square} - 4 \times A_3 \ldots\ldots\ldots\ldots\ldots\ldots\ldots\ldots\ldots\ldots\ldots\ldots\ldots\ldots\ldots\ldots\ldots\ldots\ldots\ldots\ldots\ldots [8]$$

Similarly, the area of triangular pore between three particles with round neck ($A_{\text{round neck, }\Delta}$) is given by Eq. 9.

$$A_{round\ neck,\ \text{tri}} = A_{sharp\ neck,\ \Delta} - 3 \times A_3 \ldots\ldots\ldots\ldots\ldots\ldots\ldots\ldots\ldots\ldots\ldots\ldots\ldots\ldots\ldots\ldots\ldots\ldots\ldots\ldots\ldots [9]$$

Perimeter is an important parameter of geometries used to quantify the morphological parameters of a pore. It is defined as the total length or circumference of the pore. For the pore with a sharp neck (square and rectangular), the total perimeter is the sum of the arc length of four sectors (with radius R/r) shared by the pore area. The perimeter of the pore with a rounded neck is determined by subtracting the perimeter of a shaded area (A_3) from the perimeter of the pore with a sharp neck [1].

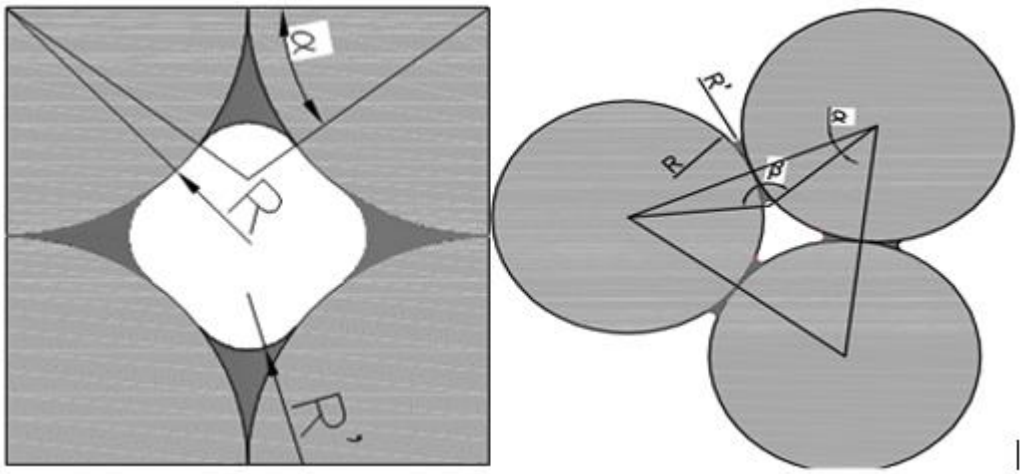

Figure 2.6 square and triangular pore angle geometry

$$\alpha = R\cos\left(\frac{R}{R+R'}\right) \ldots\ldots\ldots\ldots\ldots\ldots\ldots\ldots\ldots\ldots\ldots\ldots\ldots\ldots\ldots\ldots\ldots\ldots\ldots\ldots\ldots\ldots\ldots [10]$$

$$\beta = R\cos(1 - 2\times(\frac{R'}{R+R'}\times\frac{R'}{R+R'})) \ldots\ldots\ldots\ldots [11]$$

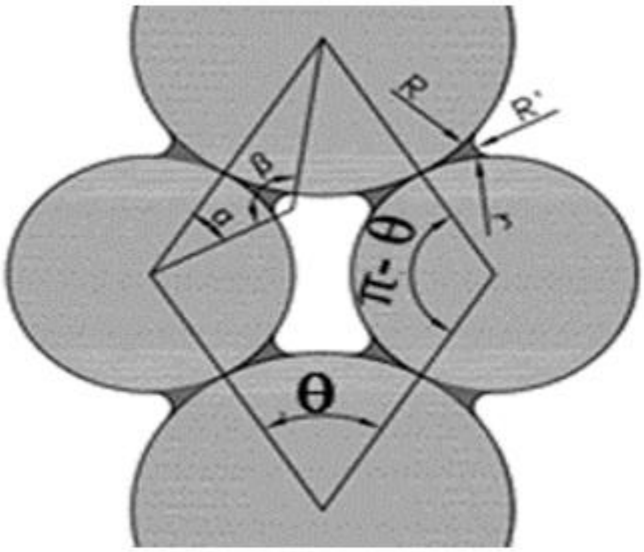

Figure 2.7 rectangular pore angle geometry

$$\theta = R\cos[\frac{(R+\frac{H}{2})}{(R+r)}] \ldots\ldots\ldots\ldots [12]$$

$$\alpha = R\cos[\frac{((r(r+R)+R'(R-r))}{((R+r)\times(r+R'))}] \ldots\ldots\ldots\ldots [13]$$

$$\beta = R\cos[\frac{(R'(R'+R)+r(R-R'))}{((R+R')\times(r+R'))}] \ldots\ldots\ldots\ldots [14]$$

Table 2.1 Perimeter and area of square, triangular and rectangular pore models [1]

Pore	**pore perimeter, P**	**pore area, A**
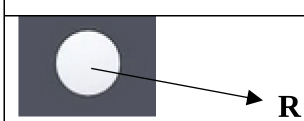	$2\pi R$	πR^2

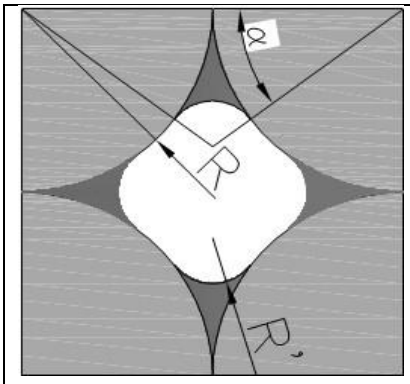	$2\pi R, \quad R' = 0$ $4\left(\frac{\pi}{2} - 2\alpha\right)R +$ $4(\pi - 2\alpha)R',$ $R' > 0$	$(4-\pi)R^2, \quad R' = 0$ $(4-\pi)R^2 - 4\left\{R\sqrt{2RR'} - \frac{R'^2(\pi-2\alpha)}{2}\right\},$ $R' > 0$
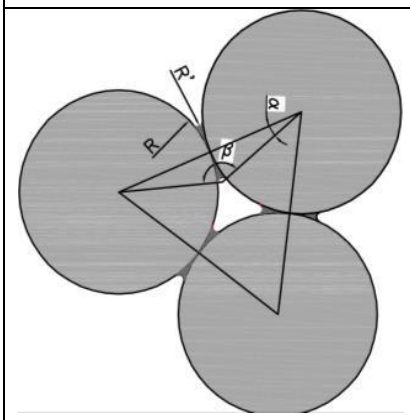	$\pi R, \quad R' = 0$ $3\left(\frac{\pi}{3} - 2\alpha\right)R + 3(\pi - 2\alpha)R',$ $R' > 0$	$\left(\sqrt{3} - \frac{\pi}{2}\right)R^2, \quad R' = 0$ $\left(\sqrt{3} - \frac{\pi}{2}\right)R^2 - 3\left\{R\sqrt{2RR' + R'^2}\right.$ $\left. - \frac{R'^2(\pi - 2\alpha)}{2} - R^2\alpha\right\},$ $R' > 0$
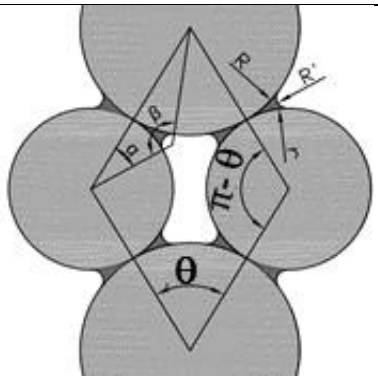	$2R\theta + 2r(\pi - \theta), \quad R' = 0$ $2R\theta + 2r(\pi - \theta) - 4r\alpha$ $-4R(\pi - \alpha - \beta)4R'\beta, R' > 0$	$2(R+r)^2\cos(\frac{\theta}{2})\sin(\frac{\theta}{2}) - r^2(\pi - \theta)$ $-R^2\theta, \quad R' = 0$ $2(R+r)^2\cos(\frac{\theta}{2})\sin(\frac{\theta}{2}) - r^2(\pi - \theta) -$ $R^2\theta - 4\{\sqrt{RrR^2(R + r + R')} -$ $\frac{R^2(\pi-\alpha-\beta)}{2} - \frac{r^2\alpha}{2} - \frac{R'^2\beta}{2}\},$ $R' > 0$

2.2.1 Pore neck curvature (R)

The sintering of powder compacts with complex-shaped particles of different sizes cannot be explained in a simple manner. However, if spherical particles of the same size are assumed, the sintering of powder compacts can be represented as the sintering between two particles. If the contact between the powder is a pint the neck curvature is sharp (R = 0). The contact between the powder is a line the neck curvature is round ($R > 0$) [26].

According to the classical model, a sharp neck is created between two perfect spherical particles (represents the initial stage of the sintering), and from the geometry, the ratio of neck to particle size is related by:

$\frac{x}{a} > 0.3$ ……[15]

Where a is the particle radius and x the neck radius.

And the radius of neck curvature r from geometry is:

$r = \frac{x^2}{2a}$ ……[16]

2.2.2 Pore size (equivalent diameter)

The diameter of the equivalent circle (D_{eq}), i.e., of the circle having the same area as the metallographic cross-section of the pore [1].

The equivalent diameter of the pore model is given by:

$$D_{eq} = 2\sqrt{\frac{A}{\pi}} \text{ ……[17]}$$

Where A, is the pore area.

3.2.3 Circularity (Pore shape)

The fraction of porosity and pore shape were measured using conventional image analysis technique.

The circularity ($0 < f_{circle} < 1$) indicates how close the shape of a pore comes to that of a circle. One measure of shape is to quantify the 'closeness' to a perfect circle [1]. For this we use the parameter Circularity which is defined as follows:

$$\boldsymbol{Circularity = 4\pi A/P^2} \text{ ……[18]}$$

Where,

A is the particle area and

P is its perimeter.

Circularity is a ratio of the perimeter of a circle with the same area as the particle divided by the perimeter.

Circularity has values in the range 0 - 1. A perfect circle has a circularity of 1 while a very 'spiky' or irregular object has a circularity value closer to 0. Circularity is sensitive to both overall form and surface roughness. Study the shapes below notice how circularity is affected by both overall form and symmetry, and surface roughness.

$f_{circle} = 4\pi A/P^2$ where A and P are the area and the perimeter, respectively, of the metallographic cross-section of the pore.

2.2.4 Fraction of Load Bearing Section

The mechanical properties of porous sintered materials may be successfully correlated to the fraction of the load bearing section and to the mechanical properties of the metallic matrix. Fraction of load bearing section can be determined from porosity and the pore morphology [10] and increases with the sintering temperature [32].

The fraction of the load bearing section (Φ) is determined as:

$$\Phi = [1 - (5.58 - 5.57 f_{circle})\varepsilon]^2 \quad \ldots\ldots [19]$$

Where ε is fractional porosity and f_{circle} *is* the pore morphology parameter.

2.3 Effect of Porosity on Material Properties

The mechanical behavior affected by porosity formation in sintered steel is focused on tensile and fatigue properties. Porosity tends to decrease the mechanical properties of sintered steel. Porosity formation which obviously depends on the matrix composition and microstructure, affects significantly the elastic modulus (E), yield strength (σ_y) and ultimate tensile strength (σ_u) of the sintered steel [6-8].

Significant research has been completed on the relationship between porosity and material properties. Models typically agree that the relationship falls into categories based on the level of porosity shape and size.

Yang and Chunhui [8]. Conducted experimental work to investigate the pore size effects on the mechanical properties and deformation behaviors of titanium foams. He fabricated cylindrical titanium foam samples with different pore sizes through powder metallurgy. pore size, pore distribution and the ratios of the length to width of pores are determined by scanning electron microscope (SEM). Compressive tests are carried out to determine the mechanical properties of the titanium foams with different pore sizes. Mechanical properties of titanium foams with pore sizes in the range of <100 and >800 μm were investigated by compressive tests focusing on the effects of pore sizes on the Young's modulus and plateau stress. Results indicated that the Young's modulus and plateau stress increase with a decrease in pore size. In particular, the specimen with the small pore size of <100 μm has the highest Young's modulus of 23 GPa and plateau stress of 80.9 MPa; while the specimen with the largest pore size of >800 μm exhibits the lowest Young's modulus of 13.6 GPa and plateau stress of 44.8 MPa.

Zeleniakienė and Kleveckas [9]. Conducted numerical finite element method to identify stress and strain state in circular porous polymer material microstructure in dependence on porosity value and mode under tensile loading by constant force of 1.33 N. The highest local stress values were found in the free surface of polymer located at the boundary with pore. Both pores size and their distribution mode influence values of the stress. The stresses and deformability increase with increasing porosity value. The lowest deformability and stress values were obtained up to material porosity 0.5. In this case influence of porosity mode on the stress and strain state is insignificant. The high material porosity greater than 0.5 and the absence of large inter pores zones cause the relatively low stress values and high deformability of material.

Liao Qiu [16]. Conducted experimental and numerical study the influence of the porosity of porous titanium on mechanical properties has with experimental and finite element analysis software of COM SOL Multiphysics and digital image analysis software of Image-J. The simulation results show that the porosity of porous titanium increases from 28.3% up to 72.3% that it results from the elastic modulus decreased from 30.77GPa to 15.94GPa. In addition, the experiment results show that the elastic modulus decreased from 32.28 GPa to 8.4 GPa. Not only the porosity has great influence on compressive properties, but the distribution of pore and microscopic porous also take effect. It shows that the elastic modulus decreases with the increase of porosity.

Zhiqiang Wei [7]. Have studied the stress field around a pore as a function of the pore position, cluster, orientation and size in depth in the surface of a linear elastic solid using finite element modeling of AA7075 Al alloy. This paper conducted larger pore causes a larger stress and strain concentration zone around it than a smaller pore. The stress and strain were further increased by tilting an elongated (ellipsoidal) pore in the surface. The stress and strain were much higher at the intercept point. The stress and strain concentrations were increased sharply with the decrease in distance between two pores in the surface, when they were within one radius apart in the direction perpendicular to the load axis.

Haolin Shuhao [10]. This study to numerically predict the effective elastic modulus of porous materials taking account of the influence of practical pores' size, shape and distribution mode of the porous titanium, the porous CoCrMo alloy and the porous tantalum, are considered in this study. It was found that the overall elastic behavior of porous materials is largely influenced by the pore shape, the pore distribution mode and the porosity. For all porous alloy elastic modulus decreases with increasing pore volume fraction. And elastic modulus increases with increasing the shape of pore circularity.

Jorge et al [37]. This paper investigated porosity in Al-SiC metal matrix composites (MMC) can be diminished; its existence is unavoidable. The purpose of this work is to study the effect of porosity on Young's modulus of SiC reinforced aluminum matrix composites. Finite element analysis is performed based on the unit cell and the representative volume element approaches. The reliability of the models is validated by comparing the numerical predictions against several experimental data ranging in lowand high-volume fractions and good agreement is found.

Rao Su [11]. This paper conducted Uniaxial tensile tests and scanning electron microscopy (SEM) experiments were carried out on the porous FeAl inter metallics (porosities of 41.1%, 44.2% and 49.3%, pore size of 15−30 μm) prepared by our research group to study the macroscopic mechanical properties and microscopic failure mechanism. The results show that the tensile σ−ε curves of the porous FeAl with different porosities can be divided into four stages: elasticity, yielding, strengthening and failure, without necking phenomenon. The elastic modulus, ultimate strength and elongation decrease with the increase of porosity. The yield strength changes very little when the difference of porosity is small.

Liam Morrissey [4]. This paper investigated the effect of porosity on elastic modulus in low-porosity materials (less than 10% porosity). It is conducted on spherical pore shape with different pore volume fraction. First, several models used to predict the reduction in elastic modulus due to porosity is compared with a compilation of experimental data to determine their ranges of validity and accuracy. The overlapping solid spheres model is found to be most accurate with the experimental data and valid between 3 and 10 percent porosity. Next, a FEM is developed with the objective of demonstrating that a macro scale plate with a center hole can be used to model the effect of micro scale porosity on elastic modulus. The FEM agrees best with the overlapping solid spheres model and shows higher accuracy with experimental data than the overlapping solid spheres model.

Jorge Karla [15]. have determined the effect of porosity on Young's modulus of SiC reinforced aluminum matrix composites. Finite element analysis is performed based on the unit cell and the representative volume element approaches. In the case of fully dense SiC particles and fully dense Al-matrix, the square and circular particles endure the same load to the volume fraction up to 11%. However, above this reinforcement content, the angular particle endures more load. Therefore, the effective elastic modulus of the MMC is independent of the morphology when the reinforcement content is lower to 11%. The elastic modulus is more sensitive to porosity in the matrix, which is a common defect in MMC. For the square or angular particles, the pore within the particle affects the load transfer mechanism in the same way to the pore located at the particle matrix interface. For the porosity at the particle–matrix interface, the contact points among the particle, matrix, and the pore acts as a stress concentrator. endure the same load to the volume fraction up to 11%. However, above this reinforcement content, the angular particle endures more load. Therefore, the effective elastic modulus of the MMC is independent of the morphology when the reinforcement content is lower to 11%.

Thomas et al [29]. This paper investigates the effect of void shape and arrangement on the effective elastic properties of porous microstructure. The characteristics of the voids are in different shapes, sizes and arrangement. Based on the results, void shape, size, and arrangement of porous microstructure were found sensitive to the elastic (homogenized) properties. Ellipsoidal shape has the highest Young's modulus, whereas the spherical shape has the highest Poisson's ratio and shear modulus. Cubical shape was the lowest for all the elastic properties.

Moreover, the formation arrangement in void cubical shape produced the highest Young's modulus and shear modulus.

Voronin Loboda [3]. This paper examines the effect of porosity and a porous structure on the mechanical properties of AD1M aluminum alloy. The pores arrangement has been selected as the types of porous structures: square, square with a pore in the center, staggered, triangular and hexagonal. The effect of pore diameter of 5 to 10 μm on the mechanical properties of the material has been studied. From this paper yield strength appear to be higher for the square arrangement of pores, than for all the other types of porous structures, but lower than for the closely packed material.

Samuel T et al [1]. Investigated analytical modeling of pore parameters of Fe-0.85Mo-0.35C to characterize equivalent diameter, circularity, and elongation of pores between the contacts of three and four grains with sharp and rounded necks were analyzed. Based on the number of contacts between grains, grain size, and neck size, a mathematical model was formulated to determine the equivalent diameter and pore parameters of circularity, equivalent diameter and elongation of the pore formed between grains.

Chawla Deng [22]. This paper investigated the microstructure and mechanical properties of sintered Fe–0.85Mo–Ni steels. A quantitative analysis of microstructure was correlated with tensile and fatigue behavior to understand the influence of pore fraction (3%, 4% and 10%) on mechanical behavior. The maximum tensile strength is recorded in 0.03 porosity and low tensile strength is recorded in 0.1 porosity. This implies that tensile strength, young's modulus, strain-to-failure, and fatigue strength all increased with a decrease in porosity.

Steels of three densities were studied i.e 7.0 g/cm3, 7.4 g/cm3, and 7.5 g/cm3. Increasing sintered density resulted in lower pore fraction, smaller average pore size, and more spherical pore shape. There is high tensile strength in 7.5 density and low tensile strength in 7.0 density.

Natasa Tomica [23]. This paper focused on establishing the correlation between the parameters describing the porosity and their influence on mechanical properties of materials based on EVA/PMMA polymer blends. Based on this analysis, a procedure for selecting a model with regular pore shape and distribution based on the actual (irregular) porous microstructure is proposed. The shear properties (modulus and strength) decreased drastically with increasing pore

diameter. Compatibilization of EVA/PMMA polymer blends with EVA-g-PMMA decreased the pore diameter and improved the mechanical properties.

The main parameter that determines the mechanical behavior of porous materials is the porosity itself. This parametric study is based on the examination of the influence of porosity on the mechanical properties of the EVA/PMMA polymer blend. The diameter of the pores was set so the distribution and number of pores were constant, and the porosity was changed in the range 30–50% (with 5% intervals). A linear dependence was observed, and with the increasing porosity by 10% (from 30% to 40%), the maximal shear stress that the material could withstand drops by 22%. where the shear properties (modulus and strength) decreased drastically with increasing pore diameter and a linear dependence was obtained for shear stress/modulus and porosity. A decrease of 22% of maximal shear stress when porosity increased by 10% suggested the importance of bulging of the material that playedthe role of decreasing the porosity of non-bearing material.

Jianjun et al [41]. Natural porous structure is extremely complex, and it is of great significance to study the macroscopic mechanical response of the representative volume element (RVE) with the microstructure of porous media. The macroscopic mechanical properties (elastic modulus, yield strength) of the RVE decrease with the increase of the porosity.

Jiang Bin [6]. This paper studies open cell aluminum foams with spherical pores synthesized by the space-holder method have been studied and mechanical properties of the foam were investigated considering its pore size and relative density. The compressive stress–strain curve increased with decrease in pore size and increase relative density.

Duosheng et al [12]. This paper investigates the existence of circular pores of grains will affect the stress distribution in the matrix. The matrix stress in the pores along the tensile direction is small, while the larger stresses appear on both sides of the pores. The pores in the composite will cause stress concentration and large plastic deformation. The change of porosity will not change the stress distribution of the matrix, but the higher the porosity, the greater the tendency of pore aggregation. The stress distribution in the matrix becomes more uneven as the pore size increases, and the large strain area of the matrix around the pores also increases.

2.4 Summery

- Sintered materials are typically characterized by residual porosity after sintering, which is quite detrimental to the mechanical properties of these materials. The nature of the porosity is controlled by several processing variables such as green density, sintering temperature and time, alloying additions, and particle size of the initial powders [14,19,20]. Porosity shape, size, position and clustering has their own effect on mechanical properties.
- The fraction, size, distribution, and morphology of the porosity have a profound impact on mechanical properties.
- The material properties of elastic modulus and yield strength decrease with increasing volume fraction.
- Tensile strength and elastic modulus increase with increasing density of powder metallurgy.
- Pore model with a sharp neck is used to determine the lower limit of circularity and a round pore approaches high circularity.
- Tensile strength, Young's modulus, strain-to-failure, and fatigue strength all increased with a decrease in porosity. The decrease in Young's modulus with increasing porosity was predicted with experimental and numerical modeling.

2.5 Gaps found from Literature

Different researchers conduct different analysis and follow different approaches to investigate and develop effect of pore on material properties. The review of literature carried out for the present study reveals that lot of experimental, analytical, and numerical studies have been conducted on effect of porosity on material properties of porous sintered matrix steel. Nevertheless, they have some limitation such as:

1. There is limited number of numerical studies conducted on the effect of pore shapes on material properties.
2. Most of the numerical papers have been investigated only in spherical and circular pore shape. However, in powder metallurgy process spherical, circular, square, rectangular,

triangular, irregular etc. pore shape is formed. Mostly circular, triangular, rectangular and irregular pore were appeared. So, only study the effect of circular and spherical pore on material properties is not realistic.

3. They do not take in to account the fraction of volume in modeling RVE microstructure; only conducts shape of pore to study its effect on material.
4. Have not been model and study the effect of pore size and shape with the material properties in finite Element Method.

CHAPTER THREE

MATERIALS AND METHODS

3.1 Materials

The Fe-Mo-C low pre-alloyed PM materials were used to study the pore characteristics. These powders compacted in double-action compaction then green compacts, sintered at 1150^0C [1]

Table 3.1 Code, nominal composition, sintering Temperature and applied treatments of the materials [1]

Material composition	Code	$T_{sint}(^0)C$	Powder grade
Fe-0.85Mo-0.35C	A85Mo	1150	Pre-alloyed

The powders were cold pressed in double uniaxial action compaction to obtain components. The green parts then sintered in a belt furnace with different belt speeds and sintering temperatures [1].

This material were pressed and sintered in an industrial facility by GKN Sinter Metals, Brunico, Italy.

Table 3.2 Density, poisons ratio, young's modulus and porosity of the investigated materials [1]

Material	Density (g/cm^3)	Poisons ratio	Young's modulus (G_{pa})	Porosity (%)
Fe-0.85Mo-0.35C	7.4	0.28	208	8

3.2 Numerical Methodology

In numerical analysis, all pore shape is modeled in Solid work and saved as Parasolid x.t file; the total of thirteen 3D CAD models are developed with various pore size and shape with 8 % porosity and those voids are also distributed finely and randomly by using Digimat FE material modeling, which is appropriate software for developing RVE microstructure easily. The assembled RVE microstructure models are imported to Abaqus 2020, in this part all the material

constants and boundary conditions are added, meshing and optimization are done. For FEM simulation analysis Abaqus 2020 is used.

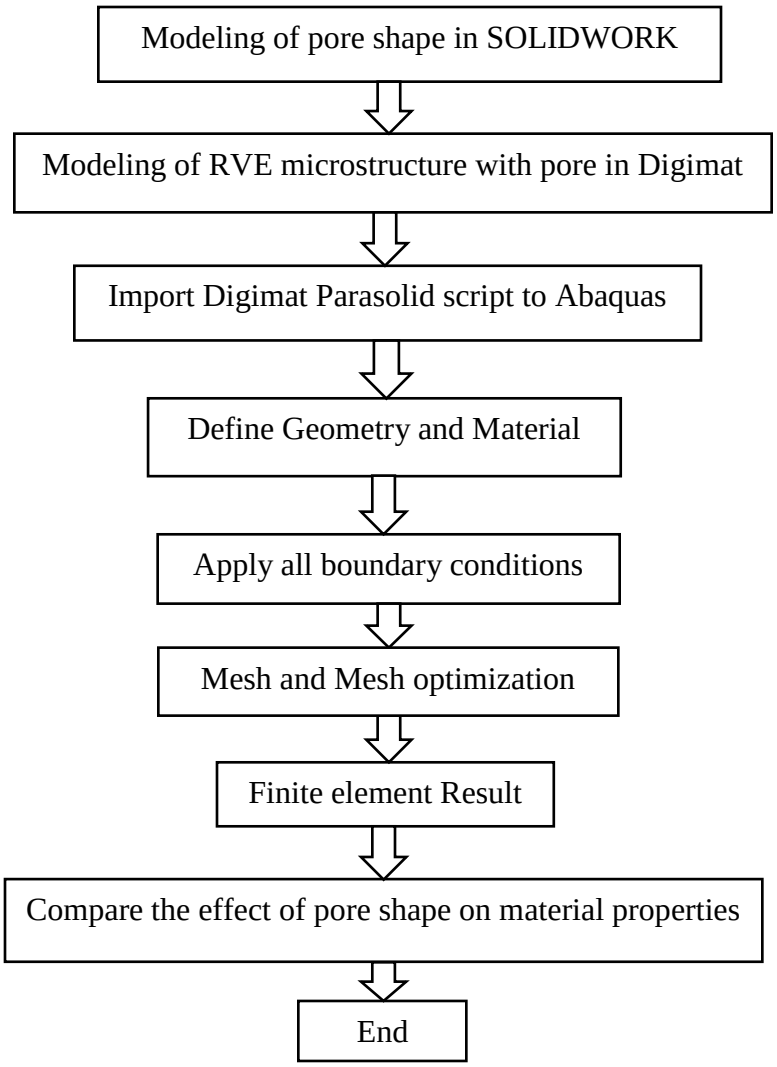

Figure 3.1 Summarized work procedure of finite element analysis

Abaqus does not identify a unit system; the operator could use a unit system randomly, as long as they are in uniformity in the analysis. The operator uses constant basic units in Abaqus.

Table 3.3 System unit in abaqus

Parameter	Units
Force/load	Newton (N)
Displacement	millimeter (mm)
Mass	Tone (10^3 kilograms)
Time	Second (S)
Stress	MPa (N/mm2)
Energy	MJ (10^{-3})
Density	$Tone/mm^3$

3.3 CAD Modeling and Finite Element Analysis

For numerical modeling process solid works, Digimat FE and Abaqus 2020 software tools are used. Mean that, the pore shape is modeled in solidwork and the RVE microstructure is modeled on DIGIMAT, finally exported to Abaqus 2020.

Digimat-FE (finite element) is the finite element-based homogenization module of Digimat which is used to model the CAD geometries of the RVE microstructure in 8 % void volume fraction.

The shape of single pore is developed in Solidwork and saves as Parasolid. The 3D representative volume element (RVE) is modeled using Digimat-FE with all the essential user-defined parameters. Then the generated microstructure geometry is imported to CAD Exchanger software to calibrate, assemble and save in Parasolid file type which is later imported in Abaqus software for further analysis.

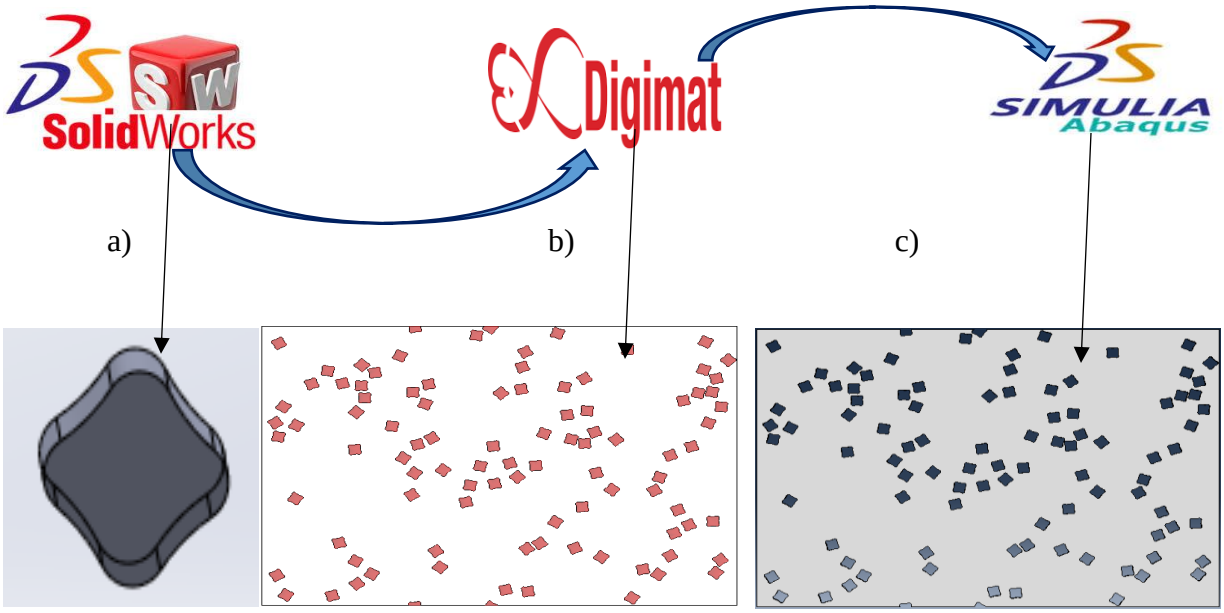

Figure 3.2 CAD modeling steps a) Solid work model b) imported into Digimat model c) imported into Abaqus model

A representative volume element (RVE) is defined if the porous material at the macroscopic scale is assumed to be homogeneous while made up of many repetitive RVEs at the microscopic scale. Then, the overall moduli of porous materials can be determined using the specific boundary excitations together with the local response of an RVE according to the micromechanics.

3.3.1 Modeling of Pore and RVE microstructure with Solidwork and Digimat

The size of the particle determined depends on the measurement technique, and particle size analysis can be achieved by any of several instruments which usually do not give equivalent determination due to difference in the measured parameters. All the particle size analyzers use one geometric parameter and assume of a spherical particle shape. It is difficult to determine the exact particle size of the powder because only the spherical particles can be defined by their diameter. Powder (particle) diameter size ranges 0.1 μm to 40 μm (9).

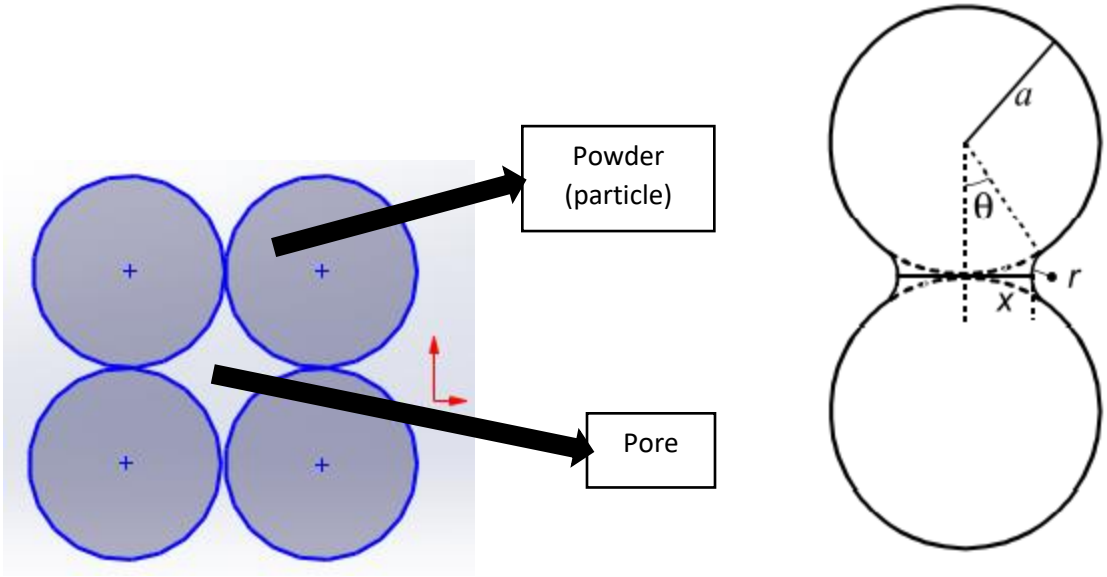

Figure 3.3 Pore model between particles and geometrical relationships

Take the average particle size ($d_{av} = \frac{40}{2} = 20\ \mu m$)

Radius of the particle is ($a = \frac{d}{2} = \frac{20}{2} = 10\ \mu m$)

The neck radius (x) is: $x > 0.3a = 0.3 \times 10 = 3$

$$\boldsymbol{x > 3}$$

The radius of curvature (r) is: $r = \frac{x^2}{2a} = \frac{3^2}{2\times10} = 0.45$

So, $\boldsymbol{r > 0.45}$

So, in this research used neck radius of curvature 0.5, 1 1nd 1.5 which is greater than 0.45.

3.3.1.1 Modeling of Square Pore and RVE Microstructure

Square geometric pore is formed between four particles (powders). The roundness of pore shape depends on the size of pore neck size. When the four particle is contact in point to each other the pore shape is sharp, and the particle is more bonded together the pore shape is more rounded.

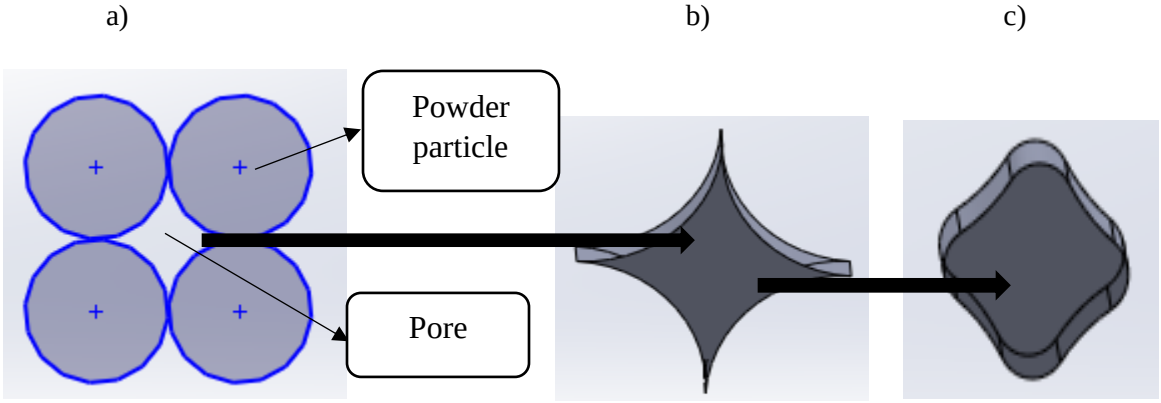

Figure 3.4 a) formation of square pore b) sharp square pore model c) round square pore model

Square pore modeled in Solidwork saved as parasolid format to import pore model to Digimat software and develop RVE microstructure model with square pore shape.

RVE microstructure with different pore shape is formed by selection of phase 1 matrix and phases 2 void and assign 8 percent of porosity in volume fraction in percent. Then select different size of square pore modeled in Solidwork and assign in inclusion CAD file in shape parameter.

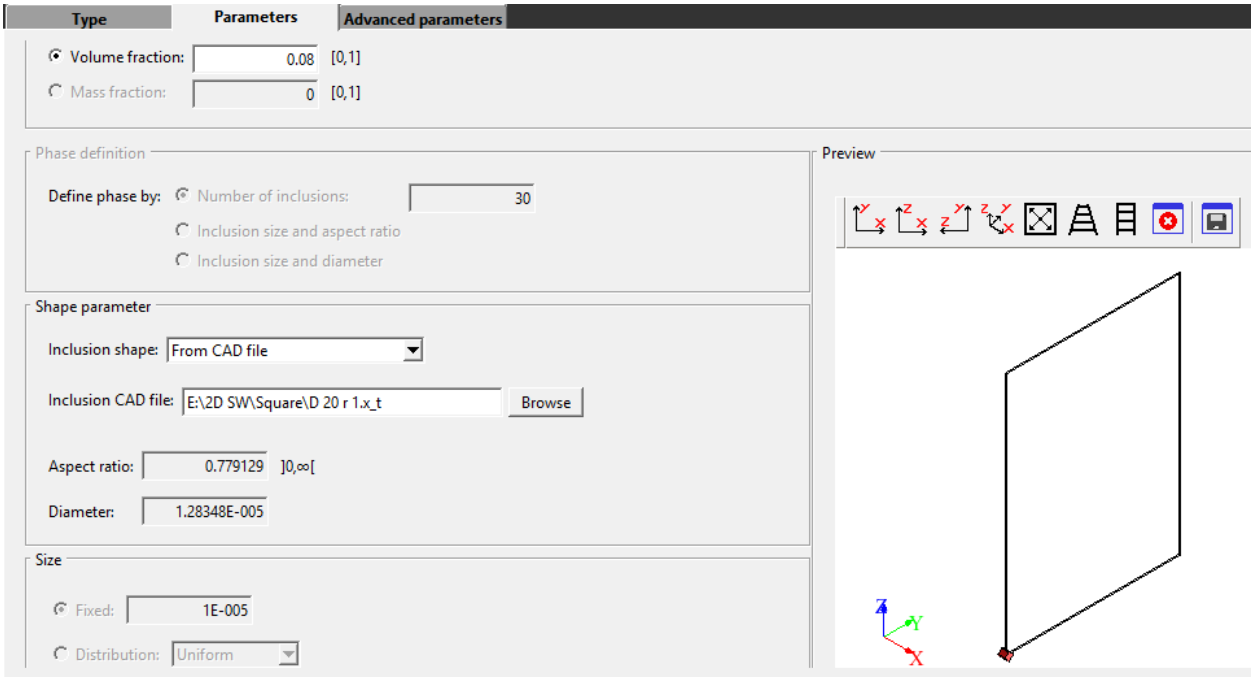

Figure 3.5 square pore RVE microstructure phase formation parameters

Model of 8% porosity size RVE microstructure of square pore shape geometry formation in DIGIMAT MSc software with different pore neck size (r) are developed in figure 3.6.

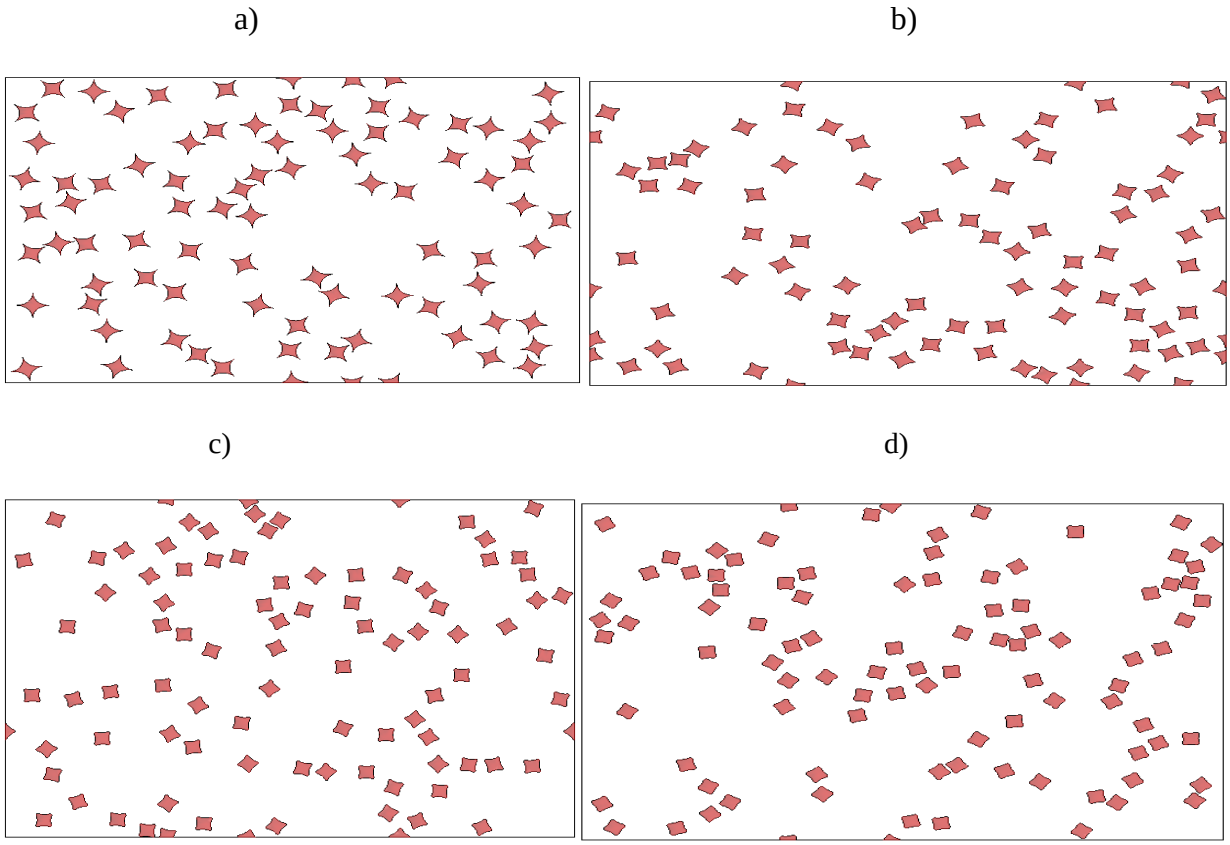

Figure 3.6 Models Representation of RVE with 8% square pore, at neck radius curvature of: a) sharp ($r = 0.5$) b) $r = 0.5$ c) $r = 1$ and d) $r = 1.5$

3.3.1.2 Modeling of Triangular Pore and RVE Microstructure

Triangular geometric pore is formed between three particles (powders). When the three particle is contact in point to each other the pore shape is sharp, and the particle is more bonded together the pore shape is more rounded.

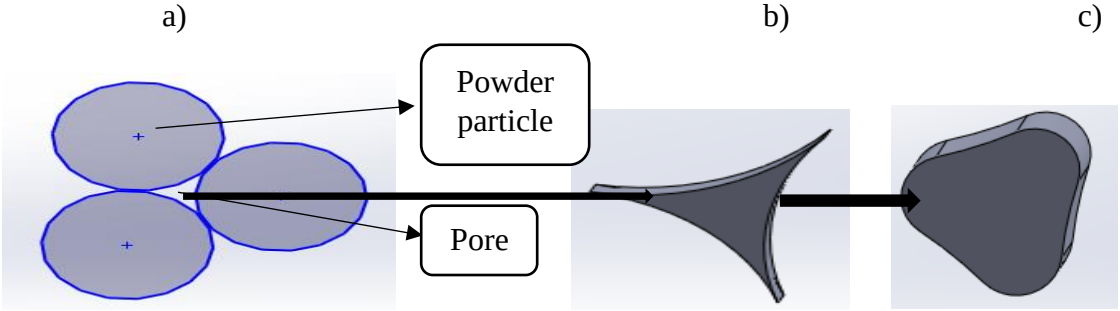

Figure 3.7 a) formation of triangular pore b) sharp triangular pore model c) round triangular pore model

Triangular pore modeled in SOLIDWORK saved as parasolid format to import pore model to Digimat software and develop RVE microstructure model with triangulare pore shape.

RVE microstructure with different pore shape is formed by selection of phase 1 matrix and phases 2 void and assign 8 percent of porosity in volume fraction in percent. Then select different size of triangular pore modeled in Solidwork and assign in inclusion CAD file in shape parameter.

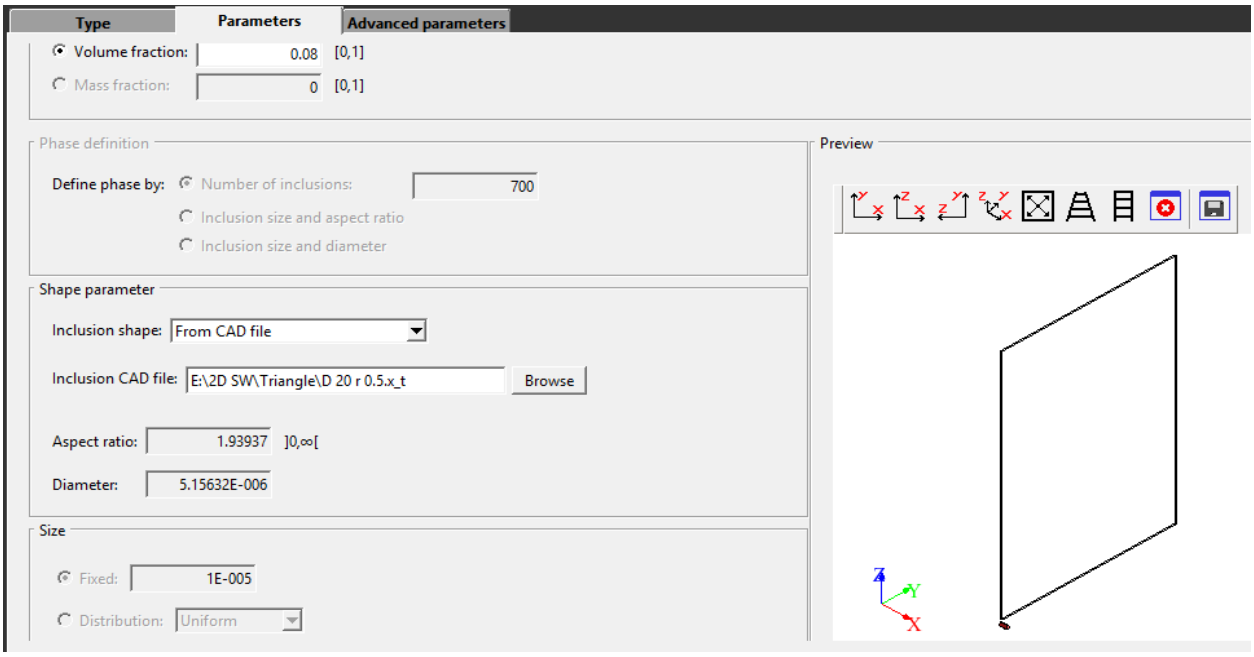

Figure 3.8 triangular pore RVE microstructure phase formation parameters

Model of 8% porosity size RVE microstructure of triangular pore shape geometry formation in DIGIMAT MSc software with different pore neck size (r) are developed in figure 3.9.

a) b)

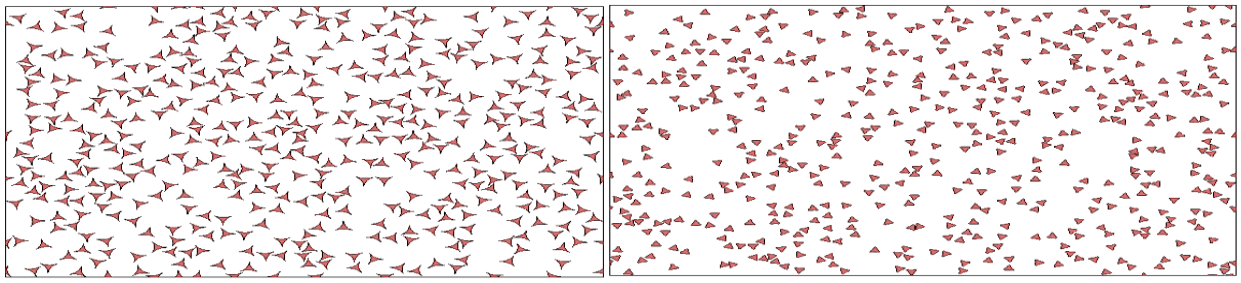

c) d)

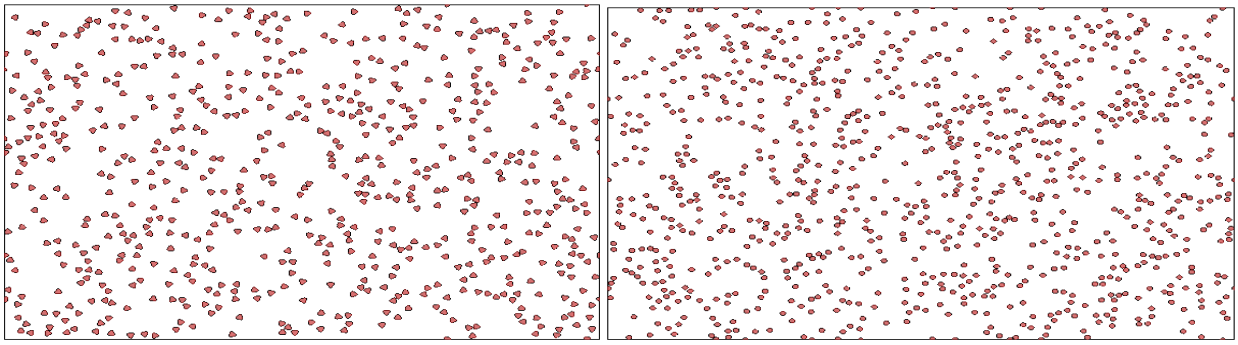

e)

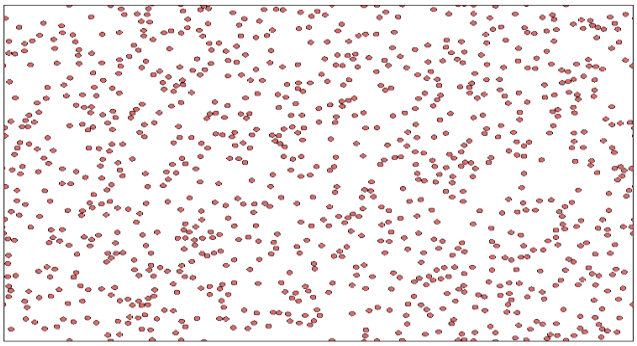

Figure 3.9 Models Representation of RVE with 8% triangular pore, at neck radius curvature of: a) sharp ($r = 0.5$) b) $r = 0.5$ c) $r = 1$ d) $r = 1.5$ and e) circular

3.3.1.3 Modeling of Rectangular Pore and RVE Microstructure

Rectangular geometric pore is formed between four different particles (powders) diameter sizes. When the four particle is contact in point to each other the pore shape is sharp, and the particle is more bonded together the pore shape is more rounded.

a) b) c)

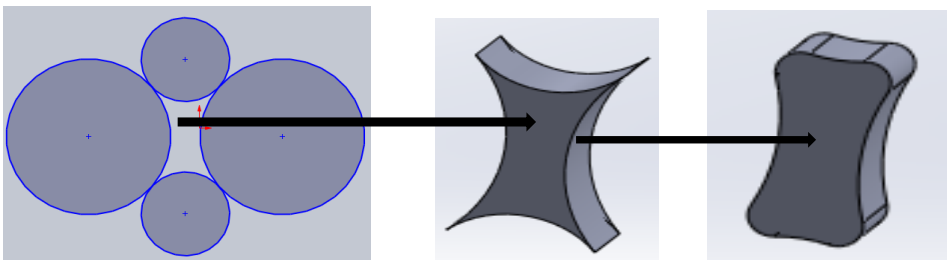

Figure 3.10 a) formation of rectangular pore b) sharp rectangular are pore model c) round rectangular pore model

Rectangular pore modeled in SOLIDWORK saved as parasolid format to import pore model to Digimat software and develop RVE microstructure model with rectangular pore shape.

RVE microstructures with different pore shape is formed by selection of phase 1 matrix and phase 2 void and assign percent of porosity in volume fraction in percent. Then select different size of rectangular pore modeled in SOLIDWORK and assign in inclusion CAD file in shape parameter.

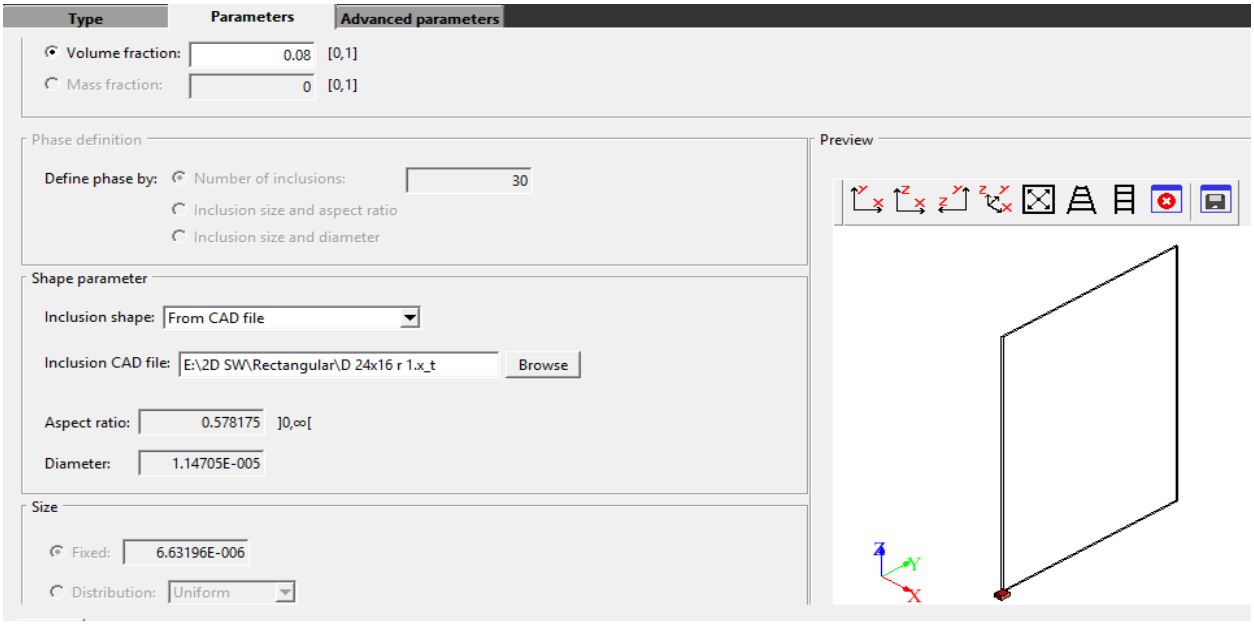

Figure 3.11 rectangular pore RVE microstructure phase formation parameters

Model of 8% porosity size RVE microstructure of rectangular pore shape geometry formation in DIGIMAT MSc software with different pore neck size (r) are developed in figure 3.12.

a) b)

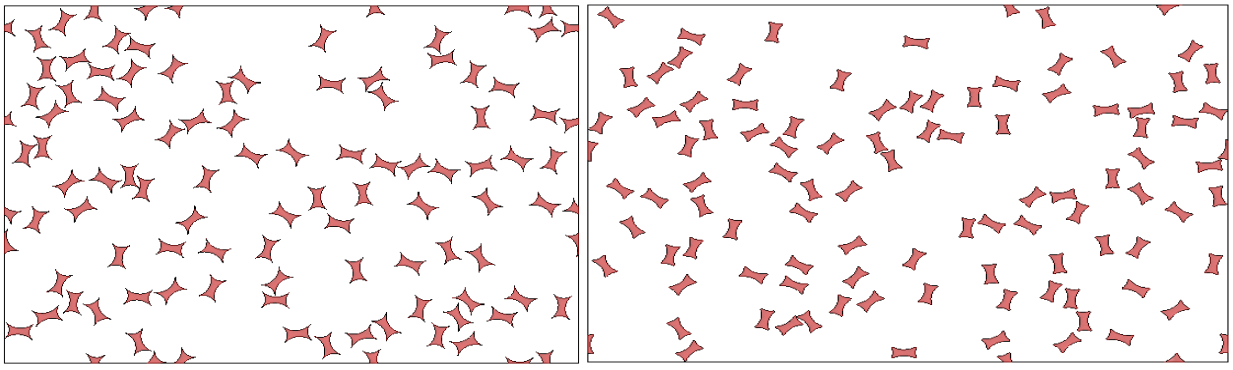

c) d)

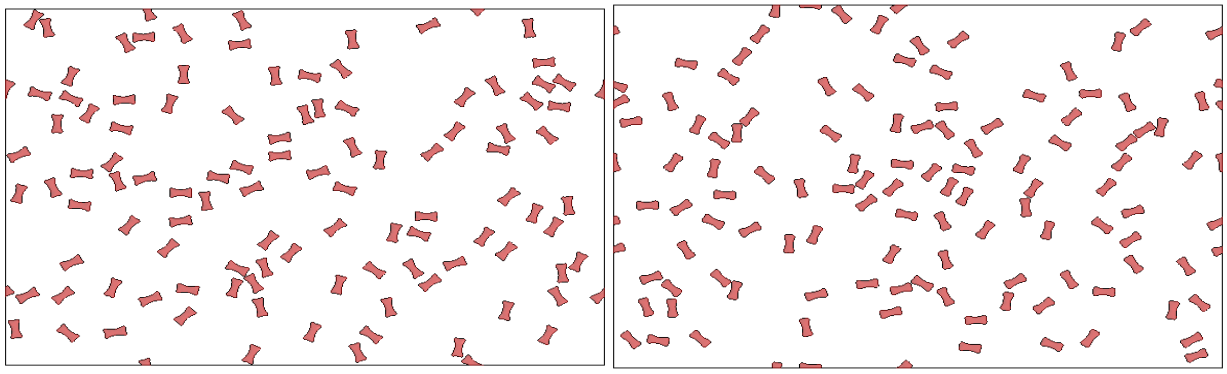

Figure 3.12 Models Representation of RVE with 8% rectangular pore, at neck radius curvature of: a) sharp ($r = 0.5$) b) $r = 0.5$ c) $r = 1$ and d) $r = 1.5$

3.3.2 Material Property Section

In the property section, material properties and body sections are assigned to specified regions of the RVE model.

Table 3.4 Material properties of RVE model

Part name	Material behavior	type	Section type
A85Mo	Elastoplastic	Isotropic	Solid, homogenous

3.3.3 Assembly Module

The assembly of this research work is RVE microstructure developed from Digimat software with 8 percent of void volume fraction and imported into Abaqus.

$r = 0$ $r = 0.5$ $r = 1$ $r = 1.5$

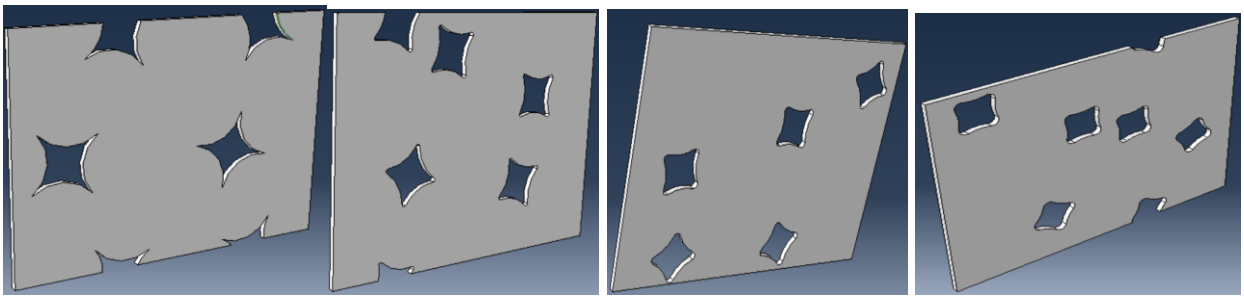

a)

$r = 0$ $r = 0.5$ $r = 1$ $r = 1.5$

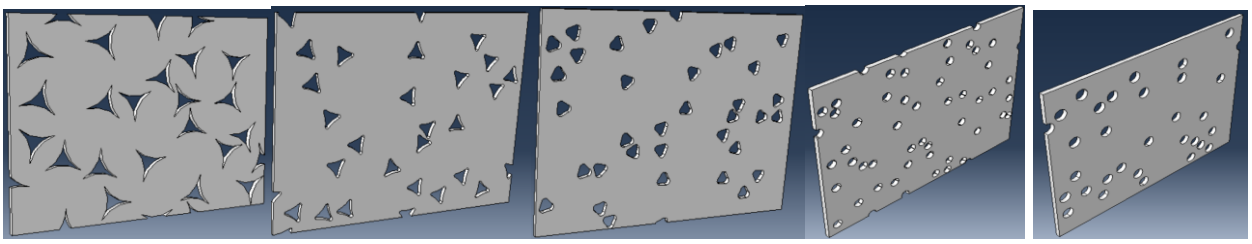

b)

$r = 0$ $r = 0.5$ $r = 1$ $r = 1.5$

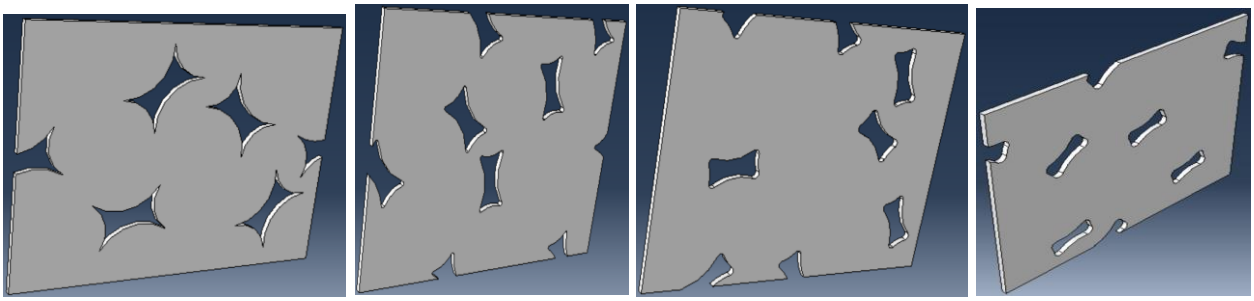

c)

Figure 3.13 Assembly of RVE microstructure model with a) square b) triangular and c) rectangular pore

Table 3.5 Finite Element Plate Specifications

Geometry	Unit
Height	60 um
Length	80 um
Thickness	2 um

3.3.4 Step Section

The step section creates a different type of steps for analyzing and useful to make single steps for each change in the model. Every step can recommend what the output parameters have to be. Also, the length of the step, the actual simulation time can be set. As well as the start, the minimum and maximum value of a single increment, and the maximum number of increments. In the initial step, the model is checked correctly, and the output requests are demanded each step is possible.

Table 3.6 Static model analysis parameters

Step	Step name	Procedure	Period	Increment size			Maximum increment
				Initial	Minimum	Maximum	
0	Initial	Initial	N/A	N/A	N/A	N/A	N/A
1	Applying load	Static general	1	0.01	0.0000015	0.1	1000

3.3.5 Boundary Condition and load Application

We define the loads and boundary conditions of the objects. Uniform distributed pressure is applied to the model in the positive Z direction. And the negative Z direction is fixed in all axis. The direct distributed load of 1 mm is applied on the surface that is opposite to the fixed surface of RVE microstructure model.

Table 3.7 Boundary and Load condition

Name	Load	BC-2
Type	Uniform	Symmetric/Antisymmetric/ encastre
Step	Step-1 (static general)	Initial
Distribution	Uniform	

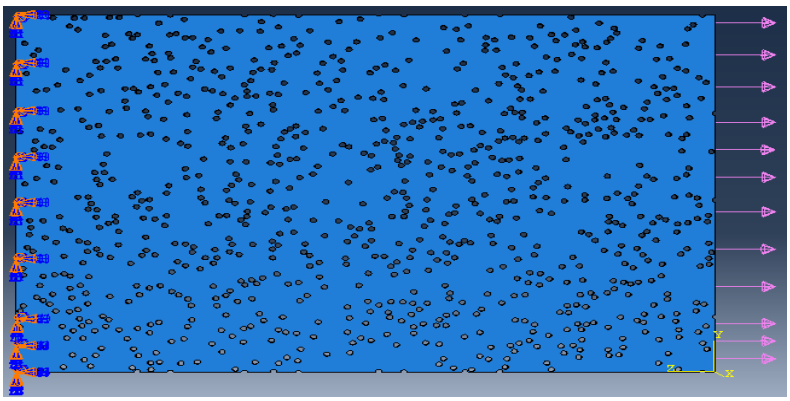

Figure 3.14 boundary and load condition

3.3.6 Meshing

A quadratic triangular mesh was employed in this simulation to conform to the many pores' nature of the RVE microstructure. A finer mesh was used in regions of pore clusters and a coarser mesh was employed in matrix-rich areas. For this study, a quadratic type element order with high smoothing quality and 0.0016-0.01 mm mesh sizes are used.

$r = 0$ $r = 0.5$ $r = 1$ $r = 1.5$

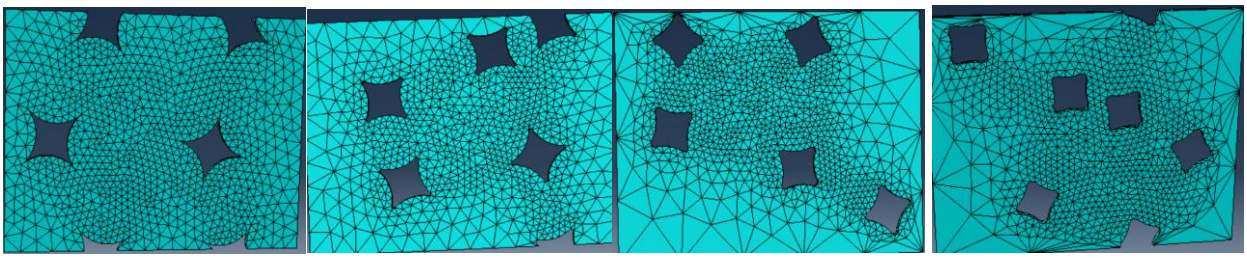

a)

$r = 0$ $r = 0.5$ $r = 1$

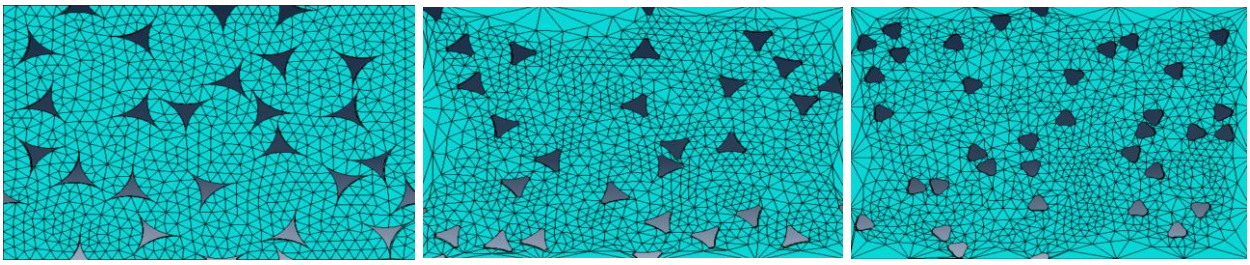

$r = 1.5$ circular

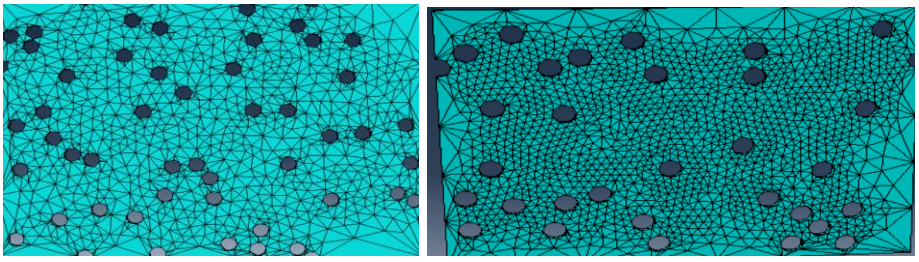

b)

$r = 0$ $r = 0.5$ $r = 1$ $r = 1.5$

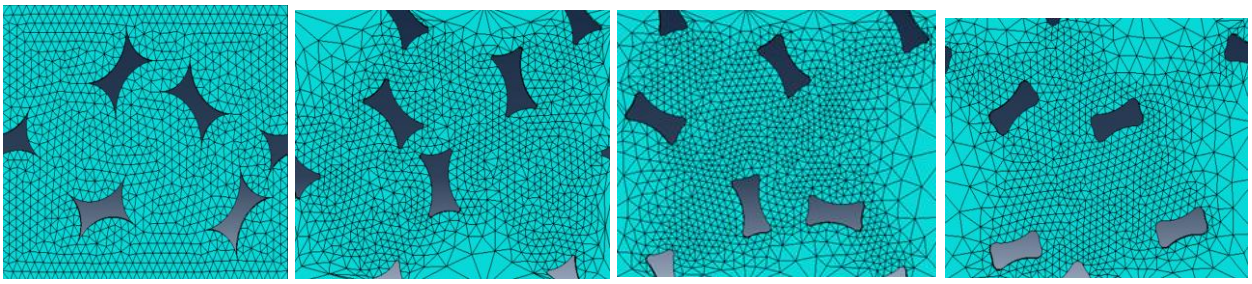

c)

Figure 3.15 Mesh modeling of RVE microstructure model with a) square b) triangular and c) rectangular pore

3.3.7 Mesh Optimization

For numerical analysis, the mesh size plays an important role. As indicated in Figure 3.17 the values of equivalent von misses stress is low for minimum mesh size and increases as mesh size increases from 0.0016 to 0.03 mm. This is because, for small volumetric element it is difficult to obtain best solution at small mesh sizes. That is because decreases up to mesh size 0.0018 mm, beyond 0.0016 mm mesh, the value of equivalent von misses stress goes constant. To check the mesh optimizations, the mesh sizes at (0.0016, 0.0018, 0.0094, 0.0095, 0.01, 0.012, 0.013and 0.0131) mm are used. These indicate that beyond 0.0016 mm, the mesh size converges as shown in the figure below. These graphs are at triangular, square, rectangular and circular model to show the patterns of mesh optimization.

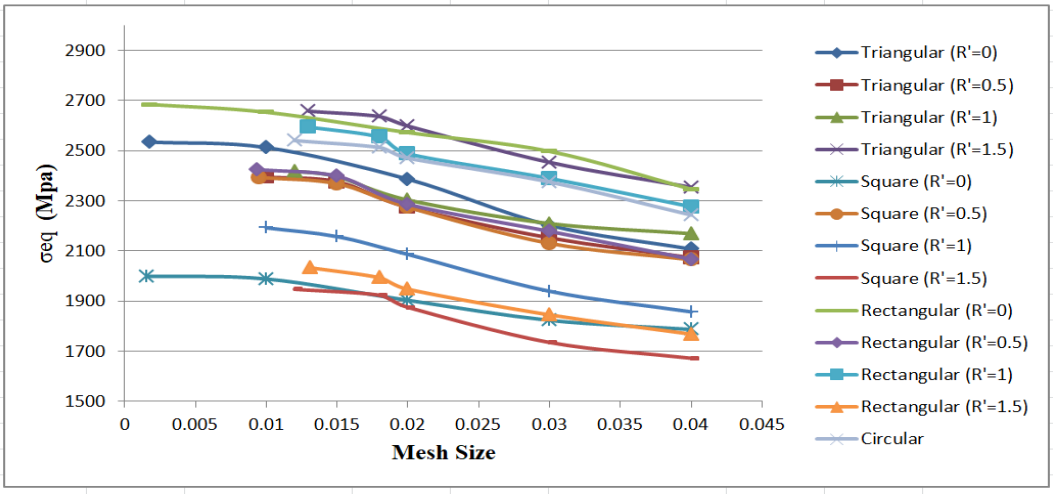

Figure 3.16 Mesh convergence analyses

For all Thirteen models, the same techniques of mesh optimization are used, mean that final equivalent von misses stress analysis is taken at the mesh size point (0.0016 – 0.03) mm at which the equivalent von misses stress values go constantly horizontal.

Table 3.8 Summary of mesh size for all models

Pore Shape model	Radius of curvature	Mesh size
Triangular	0	0.0018
	0.5	0.01
	1	0.012
	1.5	0.013
Square	0	0.0016
	0.5	0.0095
	1	0.01
	1.5	0.012
	1.75	0.012
Rectangular	0	0.0018
	0.5	0.0094
	1	0.013
	1.5	0.0131

3.3.8 Extraction of Stress and Strain

There are three approaches to extract stress and strain from finite element analysis.

1. **Localized stress strain plot.**

This is essentially about probing local points within the test specimen to assess their stress and strain plots. It will require the user to isolate an element in the model and probe its field output variables. The field output variables plotted were E11 and S11 which correspond to the strain and stress. Whilst this method is viable and quick in generating stress-strain plot, it suffers from a localization effect. If you choose a different element, you might get a different plot and so it should be used carefully.

2. Volume averaged stress strain plot.

This second approach is a better way than the previous method because it removes the localization effect on stress-strain profile seen in the previous approach. Here, the user has to identify a region within the test specimen that one wants to average-out the behavior of variables tracked in the model. It requires some prior work as you would have to identify the region, often the gauge section, and then track the history output for such region. Like the previous method, you will have to track the S11 and E11 variables (at an integration point) for all the elements that belong to that region. In the end, using the avg (X,X.) operation command in ABAQUS, we can generate the average values of stress and strain and that is our plot.

3. Experimental equivalence stress strain plot.

This third method is to extract the force and displacement profiles. To do so, the user will have to isolate a reference point where you will track the reaction force, RF1 and displacement, U1 variables in the 1- or x-axis, during the simulation. These variables are then post-processed to generate stress-strain profiles.

Volume-averaged stress-strain plot, associated over a region, is the best way to generate stress-strain plots in Abaqus.

CHAPTER FOUR

RESALT AND DISCUSSION

4.2 Finite Element Method Results

The RVE microstructure model that represents the sintering steel matrix material is analyzed in the Abaqus 2020 Simulation to study the effect of triangular, square and rectangular pore shape on material properties.

4.2.1 Effect of Pore shape on Yield Strength

There are many types of pore shape formed between contact with powder particles like square, triangular, rectangular, spherical and irregular pore shape. The stress and strain were quantified along the line perpendicular to the load axis. Computational models were constructed for each void shape for finite element analysis in Abaqus 2020.

In this study the effect of square, triangular and rectangular pore shape with different roundness on the stress and strain of sintered steels was systematically studied.

4.2.1.1 Effect of Square pore Shape on Yield Strength

$\boldsymbol{\sigma_{eq}.(M_{pa})}$ $\boldsymbol{\sigma_{eq}.(M_{pa})}$

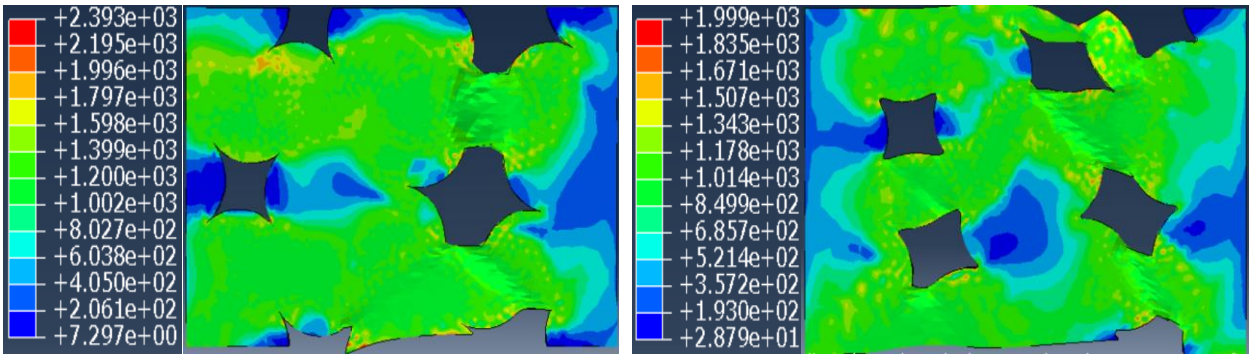

a) b)

$\boldsymbol{\sigma_{eq}.(M_{pa})}$ $\boldsymbol{\sigma_{eq}.(M_{pa})}$

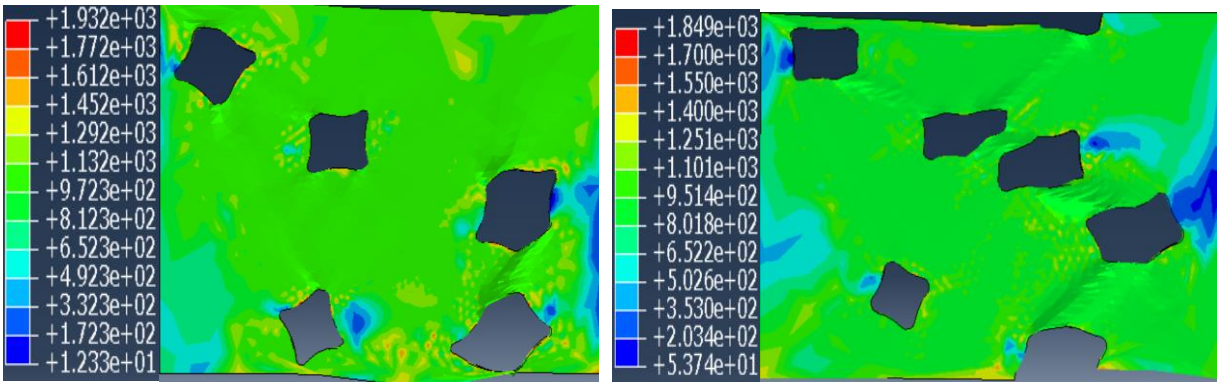

c) d)

Figure 4.1 Equivalent von mises stress distribution of square pore model circularity (f_{cir}) of a) 0.44 b) 0.56 c) 0.61 and d) 0.74

From figure 4.1 There is maximum equivalent von misses stress of 2393 M_{pa} in sharp edge square pore shape of circularity 0.44 in figure 4.1 (a) and there is low equivalent von misses stress of 1849 M_{pa} in round edge square pore shape of circularity 0.74 figure 4.1 (d). In square pore shape there is maximum equivalent von misses stress in sharp edge of pore and low equivalent von misses stress in more round edge pore. There is high distorted in interconnected pores.

A large amount of stress localization takes place in the sintered regions between pores. In particular, networks of pores are quite effective in localizing the stress in the steel ligaments between the pores. The sharpness of the pores is also important, since it has been shown that plasticity may initiate at pore edge because of the higher localized stress intensity associated with these pores.

The following result graph shows the stress vs strain for square pore Model with 8 % void fraction at circularity ($f_{cir} = 0.44$, $f_{cir} = 0.56$, $f_{cir} = 0.61$ and $f_{cir} = 0.74$).

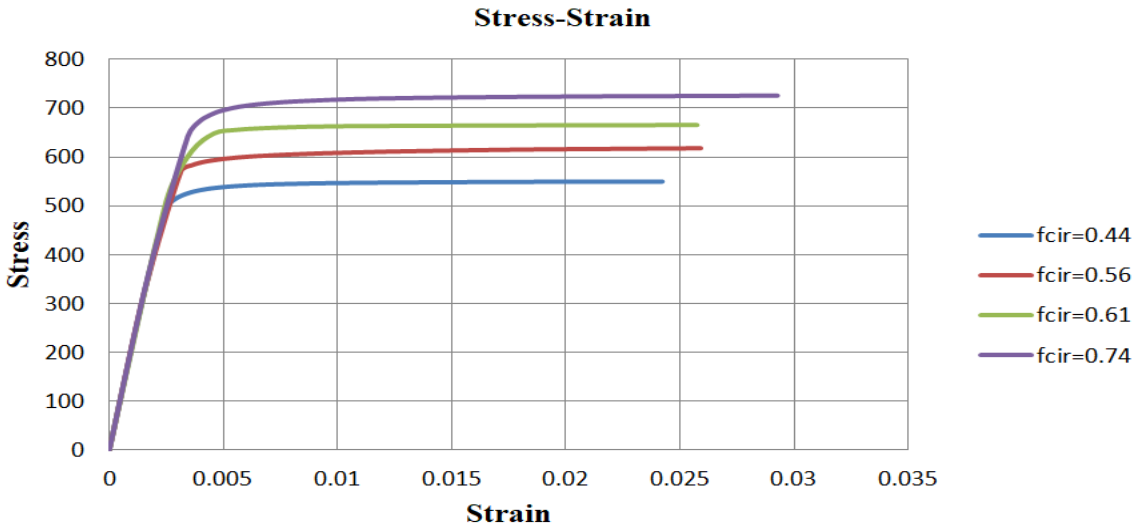

Figure 4.2 stress strain diagram of square pore model with different circularity

Figure 4.2 the stress strain is extracted using volume average stress strain plot approach. Circularity increases from 0.44 up to 0.74 with 8% porosity, resulting in that the yield strength increases from 514.75 M_{Pa} to 695.1M_{Pa}. That indicates square pore of sharpness (low circularity of 0.44) has low yield strength than round (high circularity of 0.74) pore of high circularity. The yield strength is increase with increasing circularity of square pore model.

Table 4.1 The FEM result of yield strength and elastic modulus at different square pore parameters

D (µm)	**(ε) (%)**	**R′**	**D_{eq}**	f_{circle}	**Φ**	σ_y **(M_{Pa})**	**E (G_{Pa})**
20	8	0 (sharp)	10.45	0.44	0.56	514.75	160.98
		0.5	10.28	0.56	0.65	588.65	166.4
		1	10.03	0.61	0.68	648.21	170.23
		1.5	9.76	0.74	0.78	679.23	173.76

4.2.1.2 Effect of Rectangular pore Shape on Yield Strength

$\sigma_{eq}.(M_{pa})$ $\sigma_{eq}.(M_{pa})$

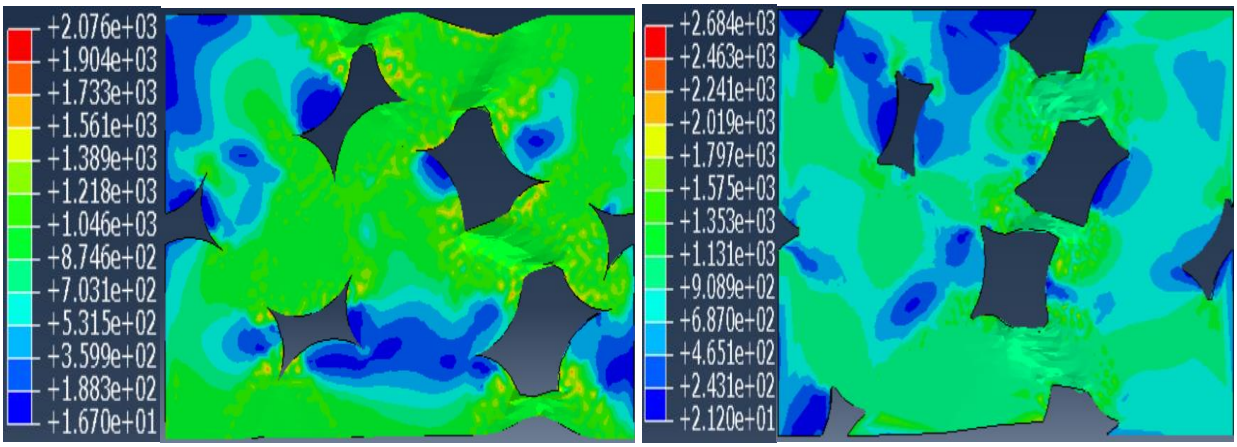

a) b)

$\sigma_{eq}.(M_{pa})$ $\sigma_{eq}.(M_{pa})$

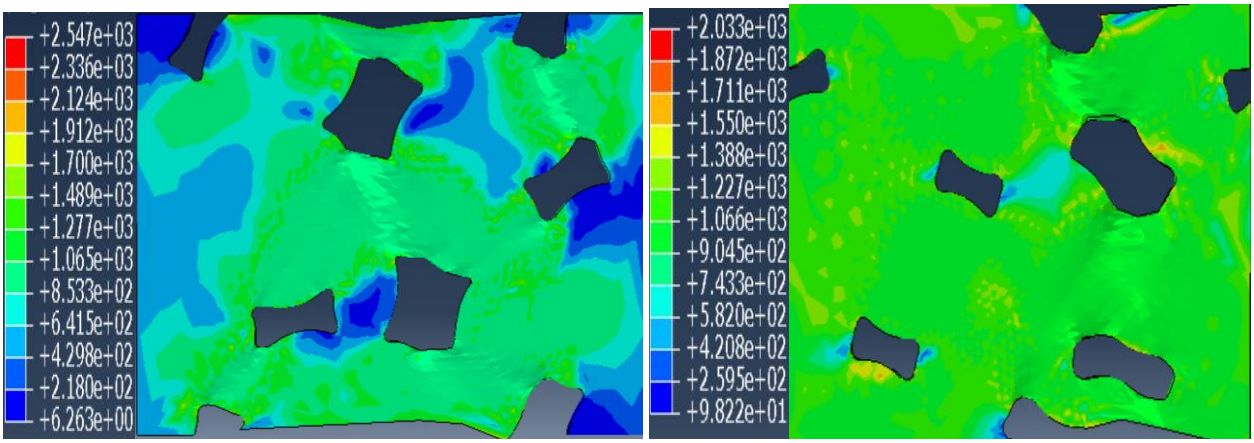

c) d)

Figure 4.3 Equivalent von mises stress distribution of rectangular pore model circularity (f_{cir}) of a) 0.25 b) 0.37 c) 0.42 and d) 0.53

From figure 4.3 There is maximum equivalent von misses stress of 2684 M_{pa} in rectangular pore shape of circularity 0.37 in figure 4.3 (b) due to distribution of pore and there is low equivalent von misses stress of 2033 M_{pa} in round edge rectangular pore shape of circularity 0.53 in figure 4.3 (d). In rectangular pore shape there is maximum equivalent von misses stress in closeness of pore and low equivalent von misses stress in more round edge pore. The distribution of the pores

is also important, since it has been shown that plasticity may initiate at pore clusters because of the higher localized stress intensity associated with these pores.

The following result graph shows the stress vs strain for rectangular pore Model with 8 % void fraction at circularity ($f_{cir} = 0.25$, $f_{cir} = 0.37$, $f_{cir} = 0.42$ and $f_{cir} = 0.53$).

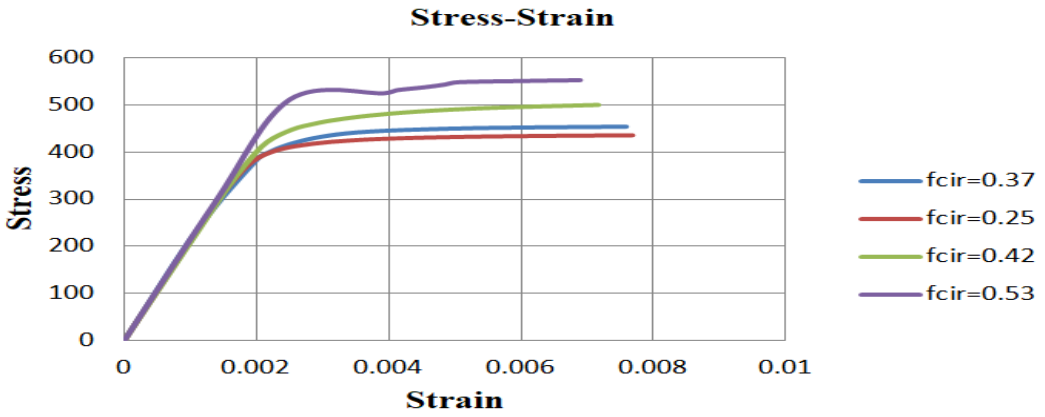

Figure 4.4 stress strain diagram of rectangular pore model with different circularity

From figure 4.4 the stress strain is extracted using volume average stress strain plot approach. Circularity increases from 0.25 up to 0.53 with 8% porosity, resulting in that the yield strength increases from 403.23 M_{Pa} to 538.04 M_{Pa}. That indicates rectangular pore of sharpness (low circularity of 0.25) has low yield strength than round (high circularity of 0.53) pore of high circularity. The yield strength is increase with increasing circularity of square pore model.

Table 4.2 The FEM result of yield strength and elastic modulus at different rectangular pore parameters

D (µm)	**R (µm)**	**ε (%)**	**R′**	**D_{eq}**	**f_{circle}**	**(Φ)**	**σ_y (M_{Pa})**	**E (G_{Pa})**
24 & 16	12 & 8	8	0 (sharp)	10.76	0.25	0.44	403.23	149.84
			0.5	10.59	0.37	0.51	424.58	153.47
			1	10.14	0.42	0.55	469.1	158.88
			1.5	9.85	0.53	0.62	538.04	162.68

4.2.1.3 Effect of Triangular pore Shape on Yield Strength

$\sigma_{eq.}(M_{pa})$

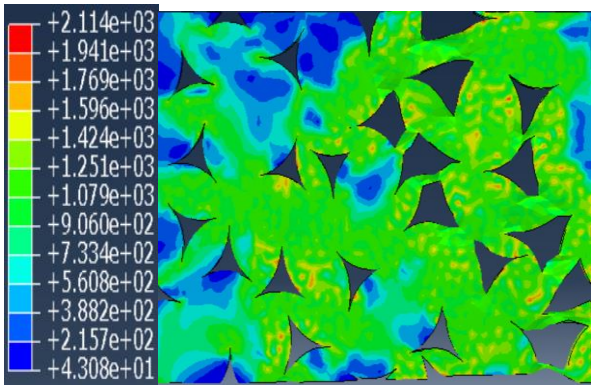

a)

$\sigma_{eq.}(M_{pa})$

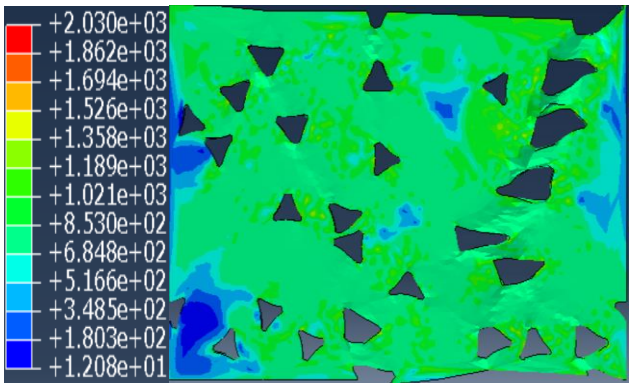

b)

$\sigma_{eq.}(M_{pa})$

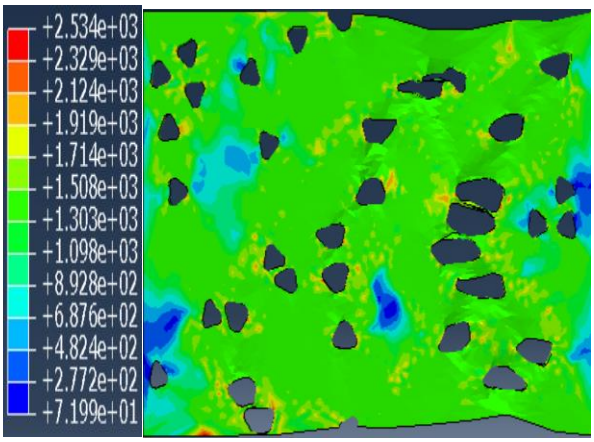

c)

$\sigma_{eq.}(M_{pa})$

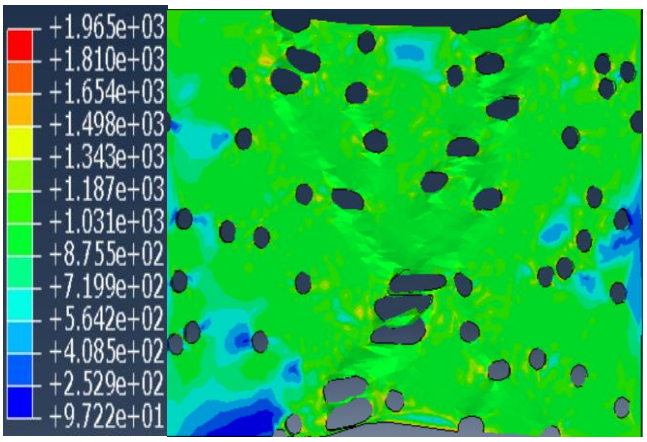

d)

$\sigma_{eq.}(M_{pa})$

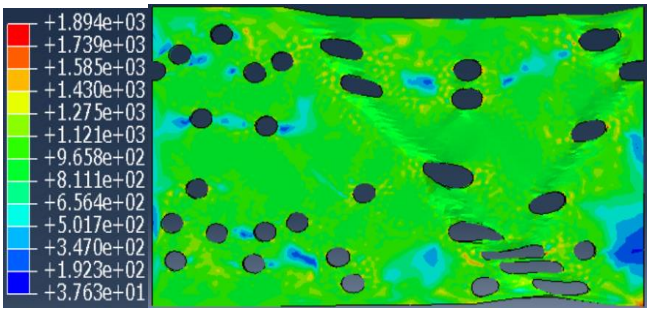

e)

Figure 4.5 Equivalent von mises stress distribution of triangular pore model circularity (f_{cir}) of a) 0.21 b) 0.60 c) 0.72 d) 0.82 and e) 1

From figure 4.5 there is maximum equivalent von misses stress of 2534 M_{pa} in triangular pore shape of circularity 0.60 in figure 4.5 (c) and there is low equivalent von misses stress of 1894 M_{pa} in triangular pore shape of circularity 1 in figure 4.5 (e). In triangular pore strength of the material is controlled by the fraction of pores, distribution of pore, position and shape. orientation, and degree of clustering of the pores. when the pores are much smaller and more homogeneously distributed, the plastic strain distribution is more uniform, and the deformation is more uniformly distributed throughout the material.

The following result graph shows the stress vs strain for triangular pore Model with 8 % void fraction at circularity ($f_{cir} = 0.21$, $f_{cir} = 0.60$, $f_{cir} = 0.72$, $f_{cir} = 0.82$ and $f_{cir} = 1$).

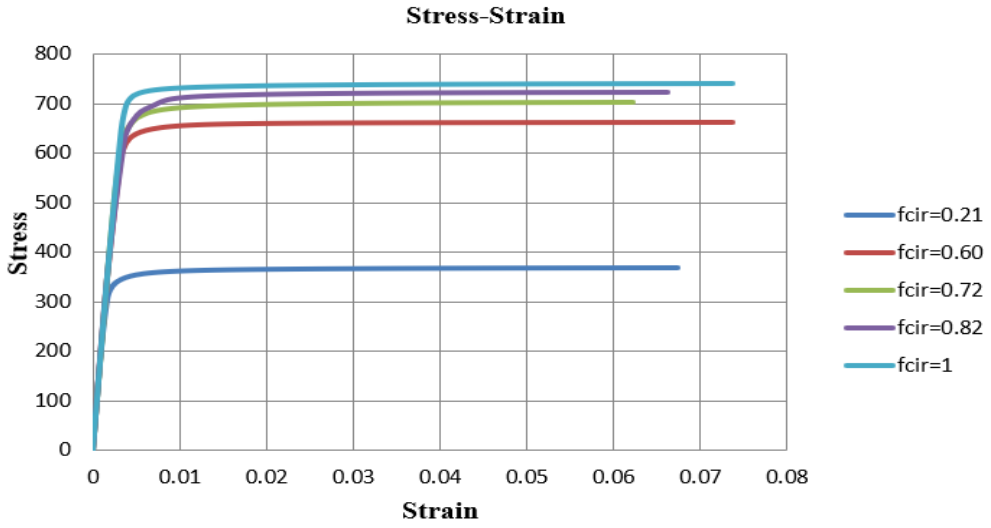

Figure 4.6 stress strain diagram of triangular pore model with different circularity

From figure 4.6 the stress strain is extracted using volume average stress strain plot approach. Circularity increases from 0.21 up to 1 with 8% porosity, resulting in that the yield strength increases from 348.55 M_{Pa} to 719.24 M_{Pa}. That indicates triangular pore of sharpness (low circularity of 0.21) has low yield strength than round (high circularity of 1) pore of high circularity. The yield strength is increase with increasing circularity of square pore model.

Table 4.3 The FEM result of yield strength and elastic modulus at different triangular pore parameters

D (µm)	R (µm)	ε (%)	R′	D_{eq}	f_{circle}	(Φ)	σ_y (M_{Pa})	E (G_{Pa})
20	10	8	0 (sharp)	4.53	0.21	0.42	348.55	147.68
			0.5	4.22	0.60	0.67	633.99	169.1
			1	3.74	0.72	0.76	664.2	171.8
			1.5	3.15	0.82	0.84	695.1	176.2
			1.75	3.11	1	0.9984	719.24	184.75

4.3 Comparison of Effect of pore shape on Yield Strength

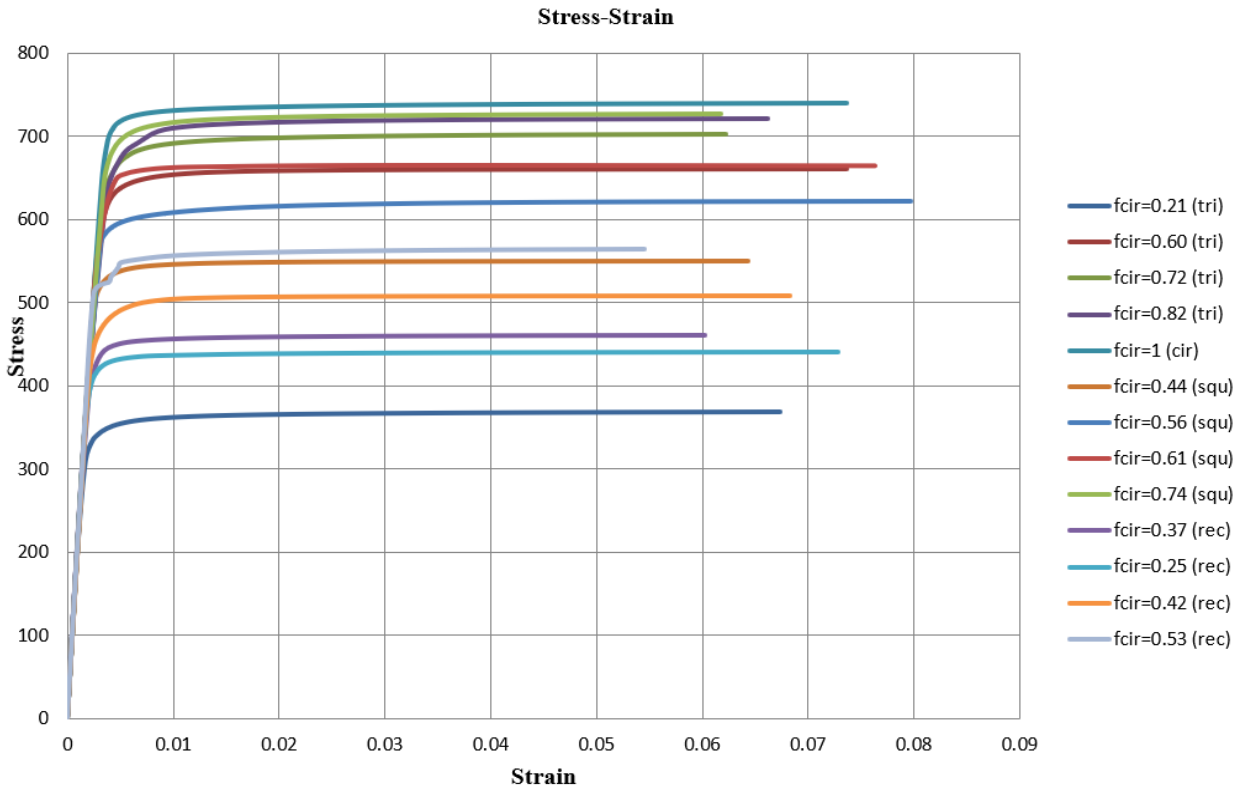

Figure 4.7 stress strain diagram of triangular, square and rectangular pore model with different circularity

The stress-strain relationships of the models with the selected 8% porosity levels of square, rectangular and circular pore are plotted in Figure 4.7. From the diagram the low circularity is 0.21 of triangular pore and the high circularity is 1 of circular pore. The low circularity 0.21

yield strength is 348.55 M_{Pa} and high circularity of 1 yield strength is 719.24 M_{Pa}. Figure 4.7 shows that in the sharp pore model triangular pore circularity of 0.21 have lowest yield strength (348.55 M_{Pa}) than square pore circularity of 0.44 yield strength (514.75 M_{Pa}) and rectangular pore circularity of 0.25 yield strength (403.23 M_{Pa}); and in the round pore model triangular pore circularity of 0.82 have high yield strength (695.1 M_{Pa}) than square pore circularity of 0.74 yield strength (679.23 M_{Pa}) and rectangular pore circularity of 0.53 yield strength (538.04 M_{Pa}). Besides the sharp pore triangular pore have high yield strength than square and rectangular pore. The displayed curves suggest a direct relationship between the circularity and the strength of the material. This relationship indicates that the low circularity voids will weaken the material as more are present in the microstructure.

4.4 Study the Effect of pore Parameter on Elastic Modulus (E)

In this study the effect of pore parameters on the effective yield strength of sintered steels was systematically studied.

4.4.1 Effect of pore neck radius of curvature (R') on Elastic Modulus (E)

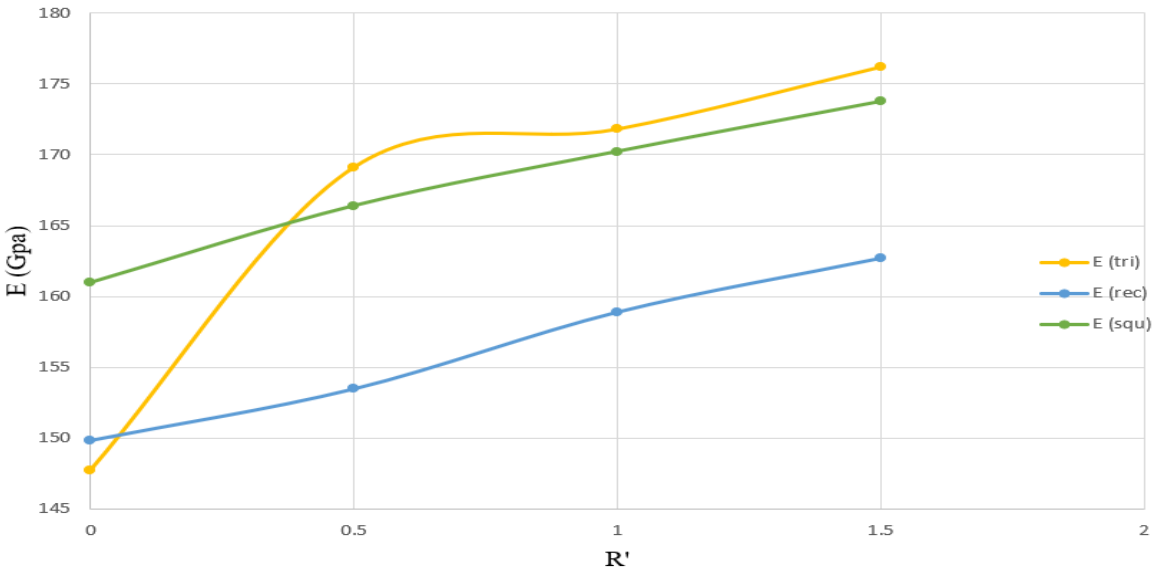

Figure 4.8 Effect of pore neck radius on elastic modulus

From figure 4.9 the lower and higher elastic is recorded in triangular pore. for all pore model (square, triangular and rectangular) there is low elastic modulus in sharp (R' = 0) model and high

elastic modulus in rounded pore model (R' = 1.5). For square, rectangle and triangle sharp edge (R'=0) elastic modulus results are 160.98 G_{pa}, 149.84 G_{pa} and 147.68 G_{pa}; and Round edge (R'=1.5) elastic modulus results are 173.76 G_{pa}, 162.68 G_{pa} and 176.2 G_{pa}.

From this analysis conclude that elastic modulus increases with increasing neck radius of curvature for square, rectangular and triangular pore shape model. For all neck radius of curvature elastic modulus of rectangular pore is lower than triangular and square pore model in RVE microstructure.

4.4.2 Effect of pore circularity (f_{cir}) on Elastic Modulus (E)

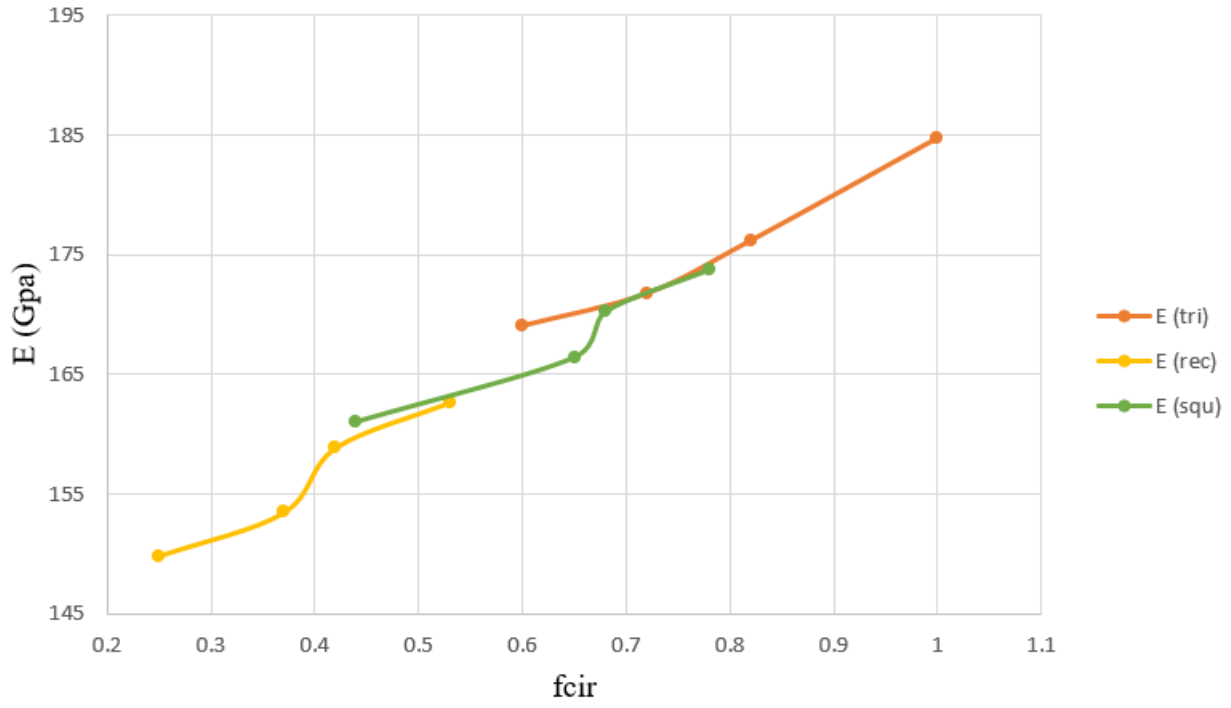

Figure 4.9 Effect of pore circularity on elastic modulus

From figure 4.9 triangular rounded pore has high elastic modulus (184.75 G_{pa}) which have high circularity of 1. And rectangular sharp pore has low elastic modulus (149.84 G_{pa}) which have low circularity of 0.25. For triangular pore when the circularity is increased from 0.60 to 1 the elastic modulus also increased from 169.1 G_{pa} to 184.75 G_{pa}. For rectangular pore when the circularity is increased from 0.25 to 0.53 the elastic modulus also increased from 149.84 G_{pa} to

162.68 G_{pa}. And square pore when the circularity is increased from 0.44 to 0.74 the elastic modulus also increased from 160.98 G_{pa} to 173.76 G_{pa}.

From this analysis we conclude that elastic modulus increases with increasing circularity for square, rectangular and triangular pore shape model. For all circularity elastic modulus of rectangular pore is lower than triangular and square pore model in RVE microstructure.

4.4.3 Effect of pore size or equivalent diameter (D_{eq}) on Elastic Modulus (E)

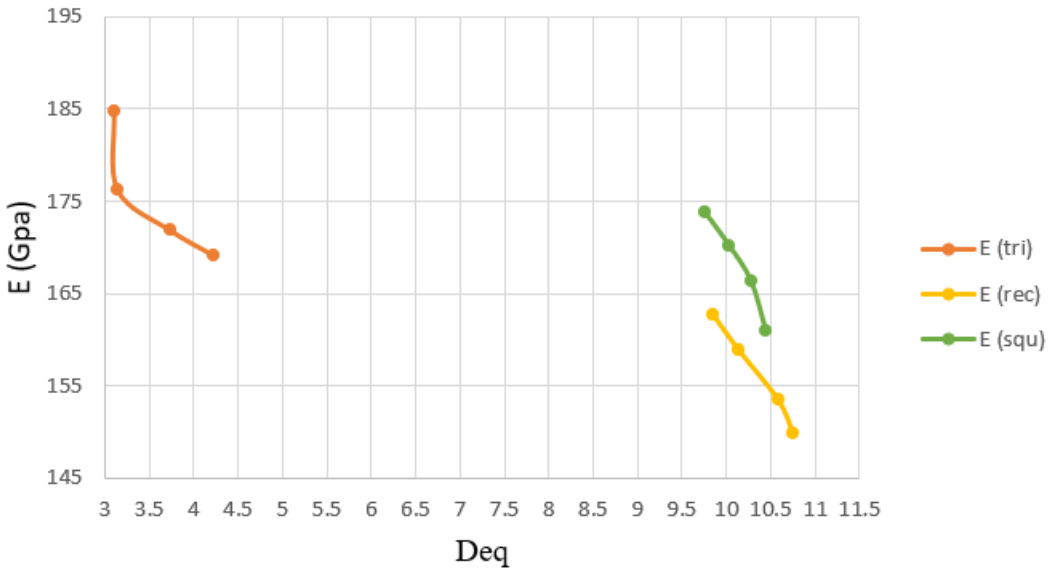

Figure 4.10 Effect of pore equivalent diameter on elastic modulus

From figure 4.10 triangular rounded pore has high elastic modulus (184.75 G_{pa}) which have low equivalent diameter of 3.11. And rectangular sharp pore has low elastic modulus (149.84 G_{pa}) which have high equivalent diameter of 10.76. For triangular pore when the equivalent diameter is increased from 3.15 to 4.53 the elastic modulus decreased from 184.75 G_{pa} to 169.1 G_{pa}. For rectangular pore when the equivalent diameter is increased from 9.85 to 10.76 the elastic modulus decreased from 162.68 G_{pa} to 149.84 G_{pa}. And square pore when the equivalent diameter is increased from 9.76 to 10.45 the elastic modulus decreased from 173.76 G_{pa} to 160.98 G_{pa}.

From this analysis we conclude that elastic modulus increases with decreasing equivalent diameter for all pore shape model. For all equivalent diameters elastic modulus of rectangular pore is lower than triangular and square pore model in RVE microstructure.

4.4.4 Effect of pore fraction of load bearing (Φ) on Elastic Modulus (E)

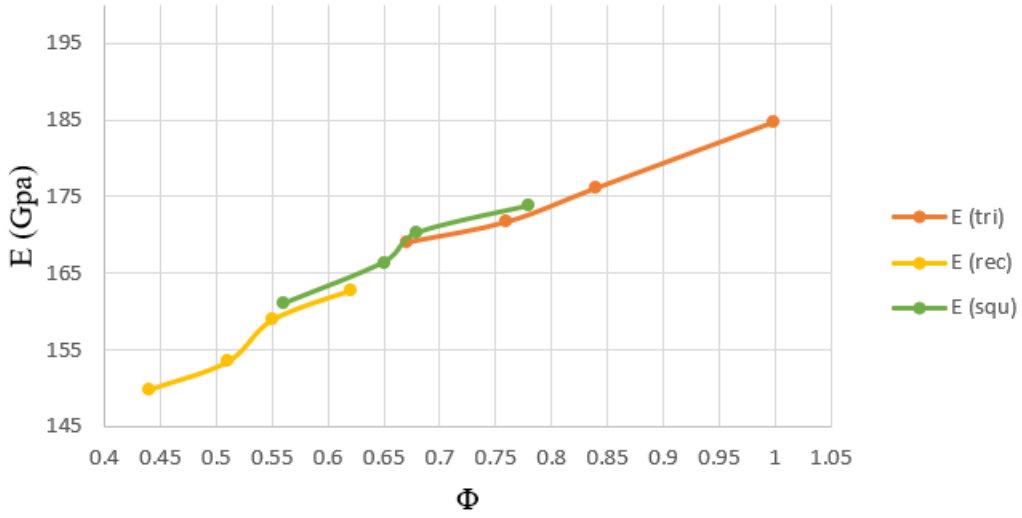

Figure 4.11 Effect of pore fraction of load bearing on elastic modulus

From figure 4.11 triangular rounded pore have high elastic modulus (184.75 G_{pa}) which have high fraction of load bearing 0.998. And rectangular sharp pore has low elastic modulus (149.84 G_{pa}) which have low fraction of load bearing 0.44. For triangular pore when the fraction of load bearing is increased from 0.67 to 0.9984 the elastic modulus also increased from 169.1 G_{pa} to 184.75 G_{pa}. For rectangular pore when the fraction of load bearing is increased from 0.44 to 0.62 the elastic modulus also increased from 149.84 G_{pa} to 162.68 G_{pa}. And square pore when the fraction of load bearing is increased from 0.56 to 0.78 the elastic modulus also increased from 160.98 G_{pa} to 173.76 G_{pa}.

From this analysis we conclude that elastic modulus increases with increasing fraction of load bearing for all pore shape model. For all fraction of load elastic modulus of rectangular pore is lower than triangular and square pore model in RVE microstructure.

CONCLUSION AND RECOMMENDATION

5.1 Conclusion

In this study the effect of pore parameters on the elastic behavior of sintered steels was systematically studied. This study was focused on effect of pore parameters (neck radius of curvature, circularity, equivalent diameter and load bearing section) on material properties of sintering steel materials. The following conclusions can be made based on the results of this study:

- Low circularity is 0.21 of triangular pore and the high circularity is 1 of circular pore. The low circularity 0.21 yield strength is 348.55 M_{Pa} and high circularity of 1 yield strength is 719.24 M_{Pa}. The sharp pore model triangular pore circularity of 0.21 have lowest yield strength (348.55 M_{Pa}) than square pore circularity of 0.44 yield strength (514.75 M_{Pa}) and rectangular pore circularity of 0.25 yield strength (403.23 M_{Pa}); and in the round pore model triangular pore circularity of 0.82 have high yield strength (695.1 M_{Pa}) than square pore circularity of 0.74 yield strength (679.23 M_{Pa}) and rectangular pore circularity of 0.53 yield strength (538.04 M_{Pa}). Besides the sharp pore triangular pore have high yield strength than square and rectangular pore. The displayed curves suggest a direct relationship between the circularity and the strength of the material.

- RVE microstructure with 8 % triangular rounded pore has high yield strength (695.1 M_{pa}) which have high circularity of 1. And rectangular sharp pore has low yield strength (403.23 M_{pa}) which have low circularity of 0.25. For triangular pore when the circularity is increased from 0.60 to 1 the yield strength also increased from 634 M_{pa} to 719.24 M_{pa}. For rectangular pore when the circularity is increased from 0.25 to 0.53 the yield strength also increased from 403.23 M_{pa} to 538.04 M_{pa}. And square pore when the circularity is increased from 0.44 to 0.74 the yield strength also increased from 514.75 M_{pa} to 679.23 M_{pa}.From this analysis we conclude that yield strength increases with increasing circularity for square, rectangular and triangular pore shape model. For all circularity yield strength of rectangular pore is lower than triangular and square pore model in RVE microstructure.

- For pore model of square, triangular and rectangular there is low elastic modulus in sharp R' = 0 (160.98 G_{pa}, 147.68 G_{pa} and 149.84 G_{pa}) and high elastic modulus in rounded pore model (R' = 1.5 (173.76 G_{pa}, 176.2 G_{pa} and 162.68 G_{pa}). Elastic modulus increases with increasing neck radius of curvature for all pore shape model.

- Triangular rounded pore has high elastic modulus (184.75 G_{pa}) which has high circularity of 1. And rectangular sharp pore has low elastic modulus (149.84 G_{pa}) which has low circularity of 0.25. The elastic modulus increases with increasing circularity for all pore shape model.

- Triangular rounded pore has high elastic modulus (184.75 G_{pa}) which has low equivalent diameter of 3.11. And rectangular sharp pore has low elastic modulus (149.84 G_{pa}) which have high equivalent diameter of 10.76. The elastic modulus increases with decreasing equivalent diameter for all pore shape model.

5.2 Recommendation to future Work

Based on the above-mentioned findings of the study following are some recommendations for future work.

1. Numerical study the effect of powder particle shape and size on mechanical properties of sintering matrix steel.
2. Numerical modeling of crack initiation or propagation analysis in finite element method.
3. Numerical simulation of sintering Temperature on mechanical properties of powder metallurgy.
4. Numerical simulation of compact pressure on mechanical properties of powder metallurgy.

Reference

[1] Samuel Tesfaye, Alberto Molinari, Solomon Mesfin "Modeling of pore parameters and experimental validation using the microstructure of 0.85Mo and 1.5Mo prealloyed sintered steels" 2021.

[2] Kubicki, B., 1995, "Stress Concentration at Pores in Sintered Materials," Powder Metal.

[3] S. V. Voronin; P. S. Loboda; M. E. Lediaev "Effect of porosity and the ordered porous structure type on the mechanical properties of aluminum materials" Mechanics, Resource and Diagnostics of Materials and Structures (MRDMS-2016); Russia. https://doi.org/10.1063/1.4967149

[4] Liam S. Morrissey and Sam Nakhla "A Finite Element Model to Predict the Effect of Porosity on Elastic Modulus in Low-Porosity Materials" The Minerals, Metals & Materials Society and ASM International 2018. doi.org/10.1007/s11661-018-4623-2

[5] A, Paknia, A. Pramanik, A. R. Dixit, and S. Chattopadhyaya, "Effect of Size, Content and Shape of Reinforcements on the Behavior of Metal Matrix Composites (MMCs) Under Tension," J. Mater. Eng. Perform., vol. 25, no. 10, pp. 4444–4459, 2016.

[6] Jiang Bin, Wang Zejuna and Zhao Naiqin, "Efect of pore size and relative density on the mechanical properties of open cell aluminum foams" 2006 Acta Materialia Inc. Published by Elsevier Ltd.

[7] HIQIANG XU, WEI WEN, and TONGGUANG ZHAI, "Effects of Pore Position in Depth on Stress/Strain Concentration and Fatigue Crack Initiation" The Minerals, Metals & Materials Society and ASM International 2011. DOI: 10.1007/s11661-011-0947-x

[8] Yang An1, Chunhui Yang, Peter Damien Hodgson1 and Cuie Wen "Effect of Pore Size on Mechanical Properties of Titanium Foams" Materials Science Forum Vols 654-656 (2010) pp 827-830.

[9] D. Zeleniakienė, T. Kleveckas, J. Liukaitis, G. Marazas, "The Influence of Porosity on Stress and Strain State of Porous Polymer Materials" material science Vol. 9, No. 4. 2003.

[10] Haolin Li, Shuhao Dong, Jiantao Liu, Yaoxiang Yu "Finite Element Modeling of Porous

Microstructures with Random Holes of Different-Shapes and -Sizes to Predict Their Effective Elastic Behavior" Appl. Sci. 2019, 9, 4536; doi:10.3390/app9214536

[11] Shu-lan SU1, Qiu-hua RAO "Effects of porosity on tensile mechanical properties of porous FeAl intermetallics" Trans. Nonferrous Met. Soc. China 30(2020) 2757−2763. DOI: 10.1016/S1003-6326(20)65418-8

[12] Duosheng Li, Shengli Song, Dunwen Zuo and Wenzheng Wu "effect of Pore Defects on Mechanical Properties of Graphene Reinforced Aluminum Nanocomposites" Metals, 2020. doi:10.3390/met10040468

[13] X. Deng , G. Piotrowski, N. Chawla, K. Narasimhan, Effect of pore clustering on the mechanical behavior of powder metallurgy (PM) steels. PM Sci Technol Briefs vol. 6, p.5–10, 2014.

[14] Pietrowski A, Biallas G. Influence of sintering temperature on pore morphology, microstructure, and fatigue behaviour of MoNiCu alloyed sintered steel. Powder Metall 1998;41(2): 109.

[15] Jorge E. Rivera-Salinas 1, Karla M. Gregorio-Jáuregui "Simulation on the Effect of Porosity in the Elastic Modulus of SiC Particle Reinforced Al Matrix Composites" Metals 2020, 10, 391; doi:10.3390/met10030391

[16] Liao, Y., Qiu, G., Bai, J.X.C. (2014). Effect of the Porosity on Compressive Properties of Porous Materials. In: TMS 2014: 143rd Annual Meeting & Exhibition. Springer, Cham. https://doi.org/10.1007/978-3-319-48237-8_55

[17] German, R. M., 1998, "Powder Metallurgy of Iron and Steel," John Wiley Sons Inc 605 Third Ave N. Y. NY 10016 USA 1998 496.

[18] Tomić, N. Z., Milanović, P., Međo, B., Vuksanović, M. M., Veljović, Đ., Rakin, M., and Jančić Heinemann, R., 2019, "Image Analysis and the Finite Element Method in the Characterization of the Influence of Porosity Parameters on the Mechanical Properties of Porous EVA/PMMA Polymer Blends," Mech. Mater., 129, pp. 1–14.

[19] Chawla, N.; Chawla, K.K. Microstructure-based modeling of the deformation behavior of particle reinforced metal matrix composites. J. Mater. Sci. 2006, 41, 913–925.

[20] Schöbel, M.; Requena, G.; Fiedler, G.; Tolnai, D.; Vaucher, S.; Degischer, H.P. Void formation in metal matrix composites by solidification and shrinkage of an AlSi7 matrix between densely packed particles. Compos. Part A Appl. Sci. Manuf. 2014, 66, 103–108.

[21] EUDIER, M., 1962, "The Mechanical Properties of Sintered Low-Alloy Steels," Powder Metall., 5(9), pp. 278–290.

[22] N. Chawla, X. Deng "Microstructure and mechanical behavior of porous sintered steels" Materials Science and Engineering A 390 (2015) 98–112.

[23] Natasa Z. Tomica , Predrag Milanovic "Image analysis and the finite element method in the characterization of the influence of porosity parameters on the mechanical properties of porous EVA/PMMA polymer blends" mechanics of materials 129 (2019).

[24] Andersson, M., 2011, "THE ROLE OF POROSITY IN FATIGUE OF PM MATERIALS," Powder Metall. Prog., (1), p. 11.

[25] Martin, W. D., Putman, B. J., and Kaye, N. B., 2013, "Using Image Analysis to Measure the Porosity Distribution of a Porous Pavement," Constr. Build. Mater., 48, pp. 210–217.

[26] Williams, S. H., and Haynes, R., 1973, "Effect of Porosity on the Fatigue Behavior of Sintered Precipitated Nickel Powder," Powder Metall., 16(32), pp. 387–404.

[27] H. Shen, S. M. Oppenheimer, D. C. Dunand, and L. C. Brinson, "Numerical modeling of pore size and distribution in foamed titanium," Mechanics of Materials, vol. 38, no. 8–10, pp. 933–944, 2006.

[28] Sun, C.; Song, M.; Wang, Z.; He, Y. Effect of particle size on the microstructures and mechanical properties of SiC-reinforced pure aluminum composites. J. Mater. Eng. Perform. 2011, 20, 1606–1612.

[29] M Thomas, K S Basaruddin, M J A Safar, S F Khan and I Ibrahim "Homogenized Properties of Porous Microstructure Effect of Void Shape and Arrangement" Journal of Physics: Conf. Series 908 (2017) 012032 doi :10.1088/1742-6596/908/1/012032.

[30] Fleck, N. A., and Smith, R. A., 1981, "Effect of Density on Tensile Strength, Fracture Toughness, and Fatigue Crack Propagation Behavior of Sintered Steel," Powder Metall.,

24(3), pp. 121–125.

[31] Andersson, M. The role of porosity in fatigue of PM materials. Powder metallurgy progress, 11.1-2 (2011)

[32] Andersson, M. Linking pore size and structure to the fatigue performance of sintered steels. World PM2010 (2010).

[33] Bergmark, A. Influence of maximum pore size on the fatigue performance of PM steel. Powder metallurgy progress 5.3 (2005).

[34] N. Chawla, D. Babic, J.J. Williams, S.J. Polasik, M. Marucci, K.S. Narasimhan, Advances in Powder Metallurgy and Particulate Materials, Metal Powder Industries Federation, 2002, p. 104

[35] Eroshkin, O.; Tsukrov, I. On micromechanical modeling of particulate composites with inclusions of various shapes. Int. J. Solids Struct. 2015, 42, 409–427.

[36] O. Prokopiev, Mechanical Properties of Porous Solids [M.S. thesis], 2009.

[37] Jorge E. Rivera-Salinas, Karla M. Gregorio-Jáuregui , José A. Romero-Serrano , Alejandro Cruz-Ramírez, Ernesto Hernández-Hernández, Argelia Miranda-Pérez and Víctor H. Gutierréz-Pérez "Simulation on the Effect of Porosity in the Elastic Modulus of SiC Particle Reinforced Al Matrix Composites" Metals 2020. doi:10.3390/met10030391

[38] Metals Handbook (1984) Powder Metallurgy, vol. 7, 9th edn, ASM International, Metals Park OH.

[39] Pavanati, H. C., Maliska, A. M., Klein, A. N. and Muzart, J. L. R., "Comparative study of porosity and pores morphology of unalloyed iron sintered in furnace and plasma reactor", Materials Research, Vol. 10, No. 1, (2007), 87-93.

[40] Kulkarni, S.G.; Achchhe, L.; Menghani, J.V. Effect of reinforcement type and porosity on strength of metal matrix composite. Int. J. Comput. Mater. Sci. Eng. 2016, 5, 1650006.

[41] Jianjun Liu, Mingyang Wu, Zhengwen Zhu, and Zuliang Shao "A Study on the Mechanical Properties of the Representative Volume Element in Fractal Porous Media" Geofluids October 2017, China. doi.org/10.1155/2017/7905218